Variation in response of C_3 and C_4 Paniceae Rubisco to temperature provides opportunities for improving C_3 photosynthesis

Robert E. Sharwood[1+], Oula Ghannoum[2+]*, Maxim V. Kapralov[3], Laura H. Gunn[1,4], and Spencer M. Whitney[1+]*.

[1] Research School of Biology, Australian National University, Canberra ACT, 2601, Australia.

[2] Hawkesbury Institute for the Environment, Western Sydney University, Richmond, New South Wales, 2753, Australia.

[+] ARC Centre of Excellence for Translational Photosynthesis, Australian National University Canberra ACT, 2601, Australia.

[3] Current Address: School of Natural Sciences and Psychology, Liverpool John Moores University, Liverpool, L3 3AF, United Kingdom

[4] Current address: Department of Cell and Molecular Biology, Uppsala University, Uppsala, SE-751 24, Sweden.

*Corresponding Authors: o.ghannoum@westernsydney.edu.au and spencer.whitney@anu.eud.au

Abstract:

Enhancing the catalytic properties of the CO_2-fixing enzyme Rubisco is a target for improving agricultural crop productivity. Here we reveal high diversity in the kinetic response between 10°C to 37°C by Rubisco from C_3- and C_4-species within the grass tribe Paniceae. The CO_2-fixation rate (k_{cat}^C) for Rubisco from the C_4-grasses with NADP-malic enzyme (NADP-ME) and phosphoenolpyruvate carboxykinase (PCK) photosynthetic pathways was two-fold greater than the k_{cat}^C of Rubisco from NAD-ME species over all temperatures. The decline in the response of CO_2/O_2 specificity with increasing temperature was slower for PCK and NADP-ME Rubisco – a trait which would be advantageous in the warmer climates they inhabit relative to the NAD-ME grasses. Variation in the temperatures kinetics of Paniceae C_3-Rubisco and PCK-Rubisco were modelled to differentially stimulate C_3-photosynthesis above and below 25°C under current and elevated CO_2. Identified are large subunit amino acid substitutions that could account for the catalytic variation among Paniceae Rubisco. Incompatibilities with Paniceae Rubisco biogenesis in tobacco however hindered their mutagenic testing by chloroplast transformation. Circumventing these bioengineering limitations is critical to tailoring the properties of crop Rubisco to suit future climates.

Concerns about how escalating climate change will influence ecosystems are particularly focused on the consequences to global agricultural productivity where increases are paramount to meet the rising food and biofuel demands. Strategies to improve crop yield by increasing photosynthesis have largely focused on overcoming the functional inadequacies of the CO2-fixing enzyme Rubisco. A competing O2-fixing reaction by Rubisco produces a toxic product whose recycling by photorespiration consumes energy and releases carbon. The frequency of the oxygenation reaction increases with temperature. To evade photorespiration many plants from hot, arid ecosystems have evolved C4 photosynthesis that concentrates CO2 around Rubisco that also facilitates improved plant water, light and nitrogen use. Here we show extensive catalytic variation in Rubisco from Paniceae grasses that align with the biochemistry and environmental origins of the different C4 plant subtypes. We reveal opportunities for enhancing crop photosynthesis under current and future CO2 levels at varied temperatures.

The realization of the dire need to address global food security has heightened the need for new solutions to increase crop yields[1]. Field tests and modelling analyses have highlighted how photosynthetic carbon assimilation underpins the maximal yield potential of crops[2]. This has increased efforts to identify solutions to enhance photosynthetic efficiency and hence plant productivity[3]. Particular attention is being paid to improving the rate at which ribulose-1,5-bisphosphate carboxylase/oxygenase (Rubisco, EC 4.1.1.39) can fix CO2 (refs 4–8). The complex structure and catalytic chemistry of Rubisco has so far made improving its performance difficult[9–11]. Diversity screens have identified natural Rubisco variants with catalytic improvements of potential benefit[11–17], but most overlook the influence of broad changes in temperature.

In C_3-plants Rubisco performance is hampered by slow CO_2-fixation rates (k_{cat}^C ~2-3 s^{-1}) and competitive O_2-fixation that produces 2-phosphoglycolate, which requires recycling by the energy-consuming and CO_2-releasing photorespiratory cycle. This necessitates C_3-plants invest up to 50% of their leaf protein (~25% of their nitrogen) into Rubisco to sustain viable CO_2 assimilation rates[1-3]. A reduction in the atmospheric CO_2:O_2 ratio during the Oligocene period (~30 million years ago) heightened plant photorespiration rates, particularly in hot, arid environments[4]. This led to the convergent evolution of C_4 photosynthesis along >65 multiple independent plant lineages[5]. C_4-plants contain a CO_2 concentrating mechanism (CCM) that allows Rubisco in the chloroplasts of bundle sheath cells (BSC) to operate under near-saturating CO_2 levels. This supresses O_2-fixation and photorespiration. The BSC CCM begins in the adjoining mesophyll cells (MC) where inorganic carbon, as HCO_3^-, is fixed to phosphoenolpyruvate (PEP) by PEP carboxylase (PEPC) to form the C_4-acid oxaloacetate (OAA). Conversion of OAA to malate (or aspartate) precedes its diffusion into the BSC where it is decarboxylated to elevate CO_2 around Rubisco. The three biochemical subtypes of C_4-plants correlate to the dominant decarboxylation enzyme: nicotinamide adenine dinucleotide (NAD) phosphate malic enzyme (NADP-ME), NAD malic enzyme (NAD-ME) or phosphoenolpyruvate carboxykinase (PEP-CK)[6,7].

An escalating appreciation of the significant kinetic variation among plant, algae and prokaryotic Form I Rubisco has, until recently, paid little consideration to the functional diversity and potential of C_4-Rubisco to improve C_3-photosynthesis [8]. Adaptation of C_4-Rubisco to elevated BSC CO_2 has beneficially increased carboxylation rate (k_{cat}^C) but unfavourably lowered CO_2-affinity (*i.e.* increased K_m for CO_2). The increase in k_{cat}^{C} endows C_4-plants with accompanying improvements in their nitrogen (less Rubisco required), water (reduced stomata apertures needed) and energy (reduced photorespiration) use efficiencies[9] – features considered of potential benefit to engineering in C_3-plants[10]. What remains unclear is the extent to which variation in the ancestral timing, CCM biochemistry and biogeographical origin has influenced the kinetic evolution C_4-Rubisco, its response to temperature and it's potential to benefit C_3-photosynthesis without a CCM.

Here we examine the diversity in the temperature response (10°C to 37°C) of Rubisco catalysis in Paniceae grasses comprising species with C_3, C_3-C_4 intermediate (C_2) and all three C_4 biochemical subtypes. We identify significant variation in the kinetic properties of Paniceae Rubisco which correlates with the photosynthetic physiology and environmental distribution of each species. We show by modelling how the potential of Paniceae Rubisco to differentially improve C_3-photosynthesis at low and high temperatures under current and future CO_2. Differences in the chaperone requirements of monocot Rubiscos are revealed that prevent use of chloroplast transformation to validate Paniceae Rubisco "catalytic switches" using the surrogate model dicot plant tobacco.

Materials and Methods

Plant Seeds and Growth Conditions

Seeds for *Panicum antidotale, P. monticola, P. virgatum, P. milliaceum, P. coloratum. P. deustum, P. milioides, P. bisulcatum, Megathyrsus maximus, Urochloa panicoides, U. mosambicensis, Cenchrus ciliaris, Setaria viridis* and *Steinchisma laxa* were obtained from Australian Plant Genetic Resources Information System (QLD, Australia) and Queensland Agricultural Seeds Pty. Ltd., (Toowoomba, Australia) (Table S1) and sown in germination trays containing a common germination mix. Three to four weeks after germination, three seedlings were transplanted into 5L pots containing potting mix and grown in the glass house under natural illumination at 28°C/22°C D/N. Plants were watered regularly with the addition of a commercial of liquid fertilizer (General Purpose, Thrive Professional, Yates, Australia).

Leaf dry matter carbon isotope composition

Leaf dry matter carbon isotope composition was determined to confirm which species use the C_4 photosynthetic pathway. Leaf discs were oven-dried then combusted in a Carlo Erba elemental analyser (Model 1108, Milan, Italy). The emitted CO_2 was analyzed by mass spectrometry (VG Isotech, Manchester, UK) and the $\delta^{13}C$ was calculated as $[(R_{sample}-R_{standard})/R_{standard}]*1000$, where R_{sample} and $R_{standard}$ are the $^{13}C/^{12}C$ ratio of the sample and the standard Pee Dee Belemnite (PDB), respectively

Rubisco catalytic measurements

Rates of $^{14}CO_2$ fixation by fully activated Rubisco were measure at 10 to 37°C using soluble leaf protein extracted from 0.5 to 2.0 cm^2 of leaf material extracted in 1 mL extraction buffer as described by Sharwood et al (2008)[11]. Preliminary assays as described in Sharwood et al., (2016) [12] were used to confirm the suitability of the extraction process for sustained maximal activity over 30 min at 25°C. The $^{14}CO_2$ fixation assays (0.5 mL) were performed in 7-mL septum-capped scintillation vials in reaction buffer (50 mM EPPES-NaOH (pH 8.19 at 25°C), 10 mM $MgCl_2$, 0.4 mM RuBP) containing varying concentrations of $NaH^{14}CO_3$ (0–40 μM) and O_2 (0–30%) (vol/vol), accurately mixed with nitrogen using Wostoff gas-mixing pumps. The vials were incubated at the appropriate assay temperature for at least 1 hr before adding 20 μL of the soluble leaf protein to initiate the reaction. The assays were terminated with 0.1 mL of 20% (v/v) formic acid after 1 min (for the assays at 25 to 37°C) or 2 min (for the assays at 10 to 20°C). The Rubisco kinetic measurements were performed using two to six biological samples (see Table S2 for detail). Each protein sample was assayed in duplicate following incubation at 25°C for 8 and 12 min. The carboxylation activity varied by <2% between each technical replicate. This confirmed each Rubisco was fully activated after incubating 8 min at 25°C with no detectable loss of activity after incubating a further 4 min. The Rubisco content (determined by ^{14}C-CABP binding[12]) and integrity of the extracted L_8S_8 holoenzyme Rubisco was confirmed by non-denaturing PAGE [13]. For each experiment a soluble leaf protein preparation was added to four assays containing the highest [$^{14}CO_2$] and 5 nmol of purified RuBP. After reacting to completion (1 to 3 h at different temperatures) they were treated with formic acid, dried and processing for scintillation counting. The measured ^{14}C cpm in each assay varied by <0.5% and the average value divided by 5 to derive the $^{14}CO_2$ specific activity. The values for pH, pK_1, pK_2 and q (the CO_2 solubility at 1 atm) used to calculate CO_2 levels in the assays at the different temperatures are provide in Table S5.

The Michaelis-Menton constants (K_m) for O_2 (K_O), for CO_2 under nitrogen (K_C) or air levels of O_2 ($K_C^{21\%O2}$) were determined from the fitted data. The maximal rate of carboxylation (V_c^{max}) was extrapolated from the fitted data and the caboxylation rate (k_{cat}^c) derived by dividing V_c^{max} by the Rubisco-catalytic site content quantified by [^{14}C]-2-CABP binding [11].

Rubisco CO_2/O_2 specificity ($S_{C/O}$) was measured using Rubisco rapidly purified by ion exchange then Superdex 200 (GE Life Sciences) size exclusion column chromatography [13]. The assays were equilibrated with 500 ppm CO_2 mixed with O_2 using Wostoff gas-mixing pumps and $S_{C/O}$ calculated using CO_2:O_2 solubility ratios of 0.033, 0.035, 0.036, 0.038, 0.039 and 0.041 at assay temperatures of 10, 15, 20, 25, 30 and 35°C, respectively (see Table S5 for gas solubility detail).

*rbc*L amplification, sequencing and phylogenetic alignment

Replica genomic DNA preparations (2 to 4) from each grass species were purified from ~0.5 cm^2 leaf discs using a DNeasy Plant Mini Kit (Qiagen) according to manufacturer's instructions. The full length *rbc*L coding sequence (including adjoining 5′UTR and 3′UTR sequence) was PCR amplified from each DNA preparation using primers 5′PanrbcL (5′-CTAATCCATATCGAGTAGAC -3′) and 3′PanrbcLDNA (5′-AGAATTACTGCATTTCGTAAC -3′). The amplified products varied in size between species (1504 to 1589–bp) but each showed identical sequence for the independent DNA preparations from each species. DNA sequences were translated into protein sequences and aligned using MUSCLE (Edgar, 2004) and the *rbc*L phylogeny reconstructed using maximum-likelihood inference conducted with RAxML version 7.2.6.

Chloroplast transformation of *Panicum rbc*L into tobacco

Plasmids pLevPdL and pLevPbL were biolistically transformed into the plastome of the tobacco genotype ^{cm}trL1 as described [13] to derive the transplastomic genotypes tob^{PdL} and tob^{PbL} that, respectively, coded the *rbc*L genes from *P. deustum* and *P. bisulcatum* (in addition to the *aad*A gene coding spectinomycin resistance) in place of the tobacco *rbc*L gene. RNA blot, [^{14}C]-2-CABP binding and PAGE analyses of Rubisco expression were performed on independent homoplasmic lines for each genotype as described above with additional experimental detail provided in Figure S7.

Statistical analysis

Statistical analysis was carried out using one-way (species or photosynthetic type/ subtype) or two-way analysis of variance, ANOVA (Statistica, StatSoft Inc. OK, USA). Means were grouped using a Post-hoc Tukey test. Detailed description of the temperature response analysis and modelling are provided in the Figure and Table legends for convenience.

Results

Our comprehensive evaluation of Rubisco kinetics within the Paniceae tribe included two C_3, one C_3-C_4 intermediate (signified C_2[7]), four NADP-ME, four PCK and three NAD-ME species (Table S1). Rubisco from tobacco, our model plant for Rubisco engineering and that commonly used in biochemical modeling, was included as a control. The C_3 and C_4 physiologies of each species were confirmed using dry matter carbon isotope ratio (δ^{13C}) measurements (Table S1). As expected, the δ^{13C} kinetic isotope effect was significantly lower in the C_2 and C_3 species (≈ -28.7‰) relative to the C_4 specie (≈ -13.3 to -14.6‰) (Fig 1a).

The carboxylation properties of Paniceae Rubisco synchronize with C_4-subtype.

Substantial variation was found in the Rubisco kinetics measured at 25°C among enzymes from C_2/C_3-species and each C_4-subtype (Table S1). Relative to the carboxylation rates (k_{cat}^{c}) of the C_2/C_3 species, the Rubisco k_{cat}^{c} was marginally higher in NAD-ME and 2-fold greater in the NADP-ME and PCK species (Fig. 1b). Consistent with the co-dependency of K_C and k_{cat}^{c} [14], greater reductions in CO_2-affinity (*i.e.* higher K_C's) were found for Rubisco from NADP-ME and PCK species relative to the NAD-ME and C_2/C_3 species (Fig 1c). Less variation was observed for the averaged oxygenation rates (k_{cat}^{O}; Fig. 1d) and O_2-affinities (K_O; Fig. 1d) among C_3 and C_4 Rubisco. Nevertheless, the NADP-ME Rubiscos tended to show less sensitivity to O_2 inhibition (*i.e.* a higher K_O). This improvement did not, however, improve the specificity for CO_2 over O_2 ($S_{C/O}$) of NADP-ME Rubisco, which was significantly lower than the more similar $S_{C/O}$ of Rubisco from the C_3, NAD-ME and PCK species (Fig 1f).

Analysis of these core catalytic parameters underscored how the strong positive correlation between k_{cat}^{c} and K_C shared by plant Rubisco [14-21] extends to Paniceae C_3- and C_4-Rubisco (Fig 1g). Uniquely, each C_4-subtype Rubisco aggregated at a distinctive position along the regression indicative of adaptation to the differences in CCM efficiencies and biogeography among C_4-subtypes[22], or reflective of differences in resource partitioning to Rubisco that, in NADP-ME plants for example, correlate with improved N-use efficiency[9]. The "subtype-grouping" of the carboxylase kinetics was not evident in the increasingly weaker linear correlations between k_{cat}^{o} and K_O (Fig 1h), k_{cat}^{c} and k_{cat}^{o} (Fig 1i) and K_C with K_O (Fig 1j). Evidently, the coordinated changes in k_{cat}^{c} and K_C for each Paniceae C_4-subtype are not tightly coupled to changes in oxygenase kinetics. This feature is common to Rubisco due to differences in the mechanism and energy profiles of the carboxylation and oxygenation reactions, a property that has facilitated the evolution of diverse Rubisco kinetics [14,23].

The potential for Paniceae Rubisco to improve C_3-photosynthesis at 25°C.

A recent study of Rubisco kinetic diversity revealed how the enzyme from some C_4-species, such as the increased $S_{C/O}$ and carboxylation efficiency under ambient O_2 (k_{cat}^{c} / $K_C^{21\%O2}$) of *Zea mays* (maize) NADP-ME Rubisco, has the potential to improve C_3-photosynthesis[8]. The bi-functionality of Rubisco necessitates consideration of both O_2 and CO_2-fixing activities when evaluating improvement within C_3-photosynthesis[1,24,25], and does not necessarily accord with a higher k_{cat}^{c}[1,8]. A correlative analysis of these parameters for Paniceae Rubisco identified a weak relationship between k_{cat}^{c} and $S_{C/O}$ ($r^2 = 0.43$; Fig 2a) supporting mounting evidence that the trade-off proposed between these parameters[14,21] shows significant natural divergence[18,26]. Differences in O_2 inhibition among the Paniceae Rubisco (*i.e.* variable K_O values, Fig 1e) resulted in $K_C^{21\%O2}$ values (quantified as $K_C(1+[O_2]/K_O)$) that showed a weaker co-dependence with k_{cat}^{c} ($r^2 = 0.76$; Fig 2b) relative to K_C ($r^2 = 0.88$; Fig 1g). This underscores the inaccuracy of using K_C measures as a proxy to interpret the relative CO_2-affinity of Rubisco under ambient O_2 (*i.e.* $K_C^{21\%O2}$).

The biochemical models of Farquhar et. al., (1980)[24] provide a useful tool to evaluate how the kinetic properties of Rubisco influence carbon assimilation in C_3-plants. These C_3-models often use tobacco Rubisco as the reference [1,8,27,28]. This stems from tobacco having well characterized Rubisco kinetics, it being the model species for bioengineering Rubisco by chloroplast and nucleus transformation, and its potential to support higher rates of photosynthesis at 25°C under low chloroplast CO_2 pressures (C_c)

than wheat Rubisco[8,29]. Figure 2c shows comparable C_3-modeling using the averaged $S_{C/O}$, k_{cat}^{c} / $K_C^{21\%O2}$ and k_{cat}^{c} values from each Paniceae biochemical subtype (Table S1). Under low C_c where CO_2-assimilation rates are carboxylase limited, Rubisco from the NADP-ME and PCK species would support higher rates of photosynthesis than the Paniceae C_3 and NAD-ME and tobacco Rubisco (Fig 2c). Under higher C_c where photosynthesis becomes limited by light dependent rates of electron transport the lower $S_{C/O}$ of the Paniceae C_4-Rubiscos would support lower rates of CO_2-assimilation relative to tobacco. In contrast the higher $S_{C/O}$ of Paniceae C_3-Rubisco would enhance their CO_2-assimilating capacity at C_c's above ~240 µbar (Fig 2c).

The temperature diversity of Paniceae Rubisco

Most diversity screens of Rubisco kinetics are undertaken at 25°C and possibly one or two other temperatures[18,20,30,31]. More rigorous studies providing kinetics that can be extrapolated over a broad temperature range have primarily focused on Rubisco from C_3-plants [15,19,28,32,33]. In general, the level of kinetic variation has been sufficient to highlight weakness in the customary use of the temperature response for tobacco Rubisco kinetics [27] to reliably model the photosynthetic responses of other species. This weakness is particularly apparent from our high precision temperature response measurements that reveal substantial kinetic diversity among Paniceae Rubisco from NAD-ME, NADP-ME, PCK and C_2/C_3 groupings (Fig 3). The parameters analyzed were $S_{C/O,}$ k_{cat}^{c} and $K_C^{21\%O2}$ (averting the need to measure K_O for C_3-modeling purposes) at six incremental temperatures between 10 and 37°C (Fig S1 to S3). The activation energies (ΔH_a) for each Rubisco parameter were comparable among the Paniceae species tested within each C_3 and C_4-subtype grouping (Table S3). This facilitated the derivation of averaged ΔH_a and scaling constant values (c) for each parameter (Fig 3a). Consistent with the highly variable properties of Rubisco from each Paniceae grouping (Fig 1) the ΔH_a values showed greater variation (Fig 3a) than that reported for Rubisco from differing C_3 species[18] and C_4-dicot *Flaveria* species[19]. This divergence is readily apparent from plots using the averaged ΔH_a values to extrapolate the temperature response of k_{cat}^{c} (Fig 3b), $K_C^{21\%O2}$ (Fig 3c), k_{cat}^{c} / $K_C^{21\%O2}$ (Fig 3d) and $S_{C/O}$ (Fig 3e) for each Paniceae Rubisco grouping and tobacco Rubisco (control).

The k_{cat}^{c} for each Rubisco showed a biphasic Arrhenius temperature response above and below ~25°C (Fig S1). This necessitated the derivation of two ΔHa and *c* measurements for each Rubisco k_{cat}^{c} (Fig. 3a) whose modeled temperature responses intersect at 25°C (Fig 3b). Importantly, the dual activation energy response of k_{cat}^{c} is universal to all temperature response studies of plant Rubisco but mostly not acknowledged[15,18-20,28,30-32]. The basis for the asymmetric response remains uncertain.

At each assay temperature the k_{cat}^{c} and $K_C^{21\%O2}$ for each NADP-ME and PCK Rubisco were consistently ~2-fold higher than Rubisco from *P. bisulcatum* (C_3), *P. milioides* (C_2) and each NAD-ME species (Table S1 and S2). The shared change in k_{cat}^{c} with temperature by NAD-ME and C_2-C_3 Rubisco (Fig 3b) was not evident in the measured $K_C^{21\%O2}$ values that showed a heightened rate of increase with temperature by NAD ME Rubisco (Fig. 3c). The biphasic response of k_{cat}^{c} was evident in corresponding measures of carboxylation efficiency (k_{cat}^{c} / $K_C^{21\%O2}$) that showed two linear responses that deviated at temperatures above and below ~25°C for each Rubisco (Fig 3d). A comparable k_{cat}^{c} / K_C temperature dependency is apparent for the Rubisco from *Flaveria* C_3 and C_4 species[19] and *Setaria viridis* C_4-Rubisco[15]. The differential slopes of the linear regression underscores the significant variation in k_{cat}^{c} and $K_C^{21\%O2}$ between each Paniceae Rubisco grouping (both below and above 25°C) and emphasizes the extrapolative limitations of kinetic surveys examining only a few temperatures. This is particularly relevant for measures of $S_{C/O}$ where the extent of exponential change appears more prevalent with reducing temperature (Fig. 3e).

The potential for improving C_3-photosynthesis under current and future CO_2 and elevated temperatures

The temperature response of each Paniceae Rubisco showed varying extents of improvement in $S_{C/O}$ and/or $k_{cat}^{c}/K_C^{21\%O2}$ relative to tobacco Rubisco (Fig S3 and S4). The improvements observed were greater for Rubisco from *P. bisulcatum* (C_3), *Urochloa panicoides* (C_4-PCK) and *P. deustum* (C_4-PCK). When modeled in a C_3-photosynthesis context under varying temperature and chloroplast CO_2 pressures (C_c) under saturating illumination (Fig S5) all three Rubiscos differentially improved carbon assimilation relative to tobacco Rubisco (Fig 4). At temperatures below 20°C the simulated photosynthesis rates were limited by electron transport rate at atmospheric CO_2 (C_a) levels above those of pre-industrial times (C_a >280 ppm ≈ C_c >170 ppm) (Fig S5). Improvements in $S_{C/O}$ were therefore required to enhance photosynthetic rates at low temperature, a kinetic trait afforded by Paniceae C_3/C_2 Rubisco (Fig 3c), in particular *P. bisulcatum* Rubisco (Fig 4 and S3). However, the heightened $S_{C/O}$ sensitivity of *P. bisulcatum* Rubisco to increasing temperature (Fig S3a) caused these improved photosynthetic rates to wane with increasing C_a and temperature (Figs 4 and S5). In contrast, the improved $S_{C/O}$ response to temperature by *P. deustum* Rubisco (Fig S3) and rising $k_{cat}^{c}/K_C^{21\%O2}$ (Fig S4) substantially improved photosynthesis rates at temperatures >20°C under current and future C_a levels (Fig 4b). This improvement exceeded that simulated for *U. panicoides* Rubisco whose lower $S_{C/O}$ hindered its enhancement potential. The antagonistic advantage of these Paniceae Rubisco to lower (*P. bisulcatum*) and higher (*U. panicoides, P. deustum*) temperatures were not apparent from the 25°C kinetic measurements.

The challenge of identifying catalytic switches in Paniceae Rubisco

The *rbc*L gene in the plastome of each Paniceae species were fully sequenced and their amino acid sequences compared (Fig 5a). A phylogenetic analysis revealed the L-subunit sequences branched according to C_3 and C_4-subtype physiology (Fig. S6) except *P. monticola* (NADP-ME) and *M. maximus* (PCK) Rubisco that share identical L-subunits but show large catalytic variation (Table S1 and S2). This suggests that Paniceae Rubisco small subunits influence catalysis, a function likely shared by the small (S-) subunits of sorghum[34] and wheat[35] Rubisco.

While examination of the S-subunit diversity among Paniceae remains to be undertaken, our L-subunit analysis identified Ala 94 and Ala 228 (spinach Rubisco numbering) as exclusive to C_4 Rubisco with Ser 328 and Glu 470 substitutions favored by PCK and NADP-ME Rubisco (Fig 5a). Potential roles for amino acids 94 and 228 in catalysis are unclear. Residue 94 is distal to the catalytic sites in the equatorial region of Rubisco exposed to solvent where it facilitates interactions with Rubisco activase (RCA)[36,37]. Residue 228 is within the α2 helix also distal to the catalytic site but proximal to residues at the interface of each L-subunit and two S-subunit βA-βB loops (Figure 5b). Ala-228-Ser substitutions influence structural movements in these loops and can influence kinetics via long range effects [38,39]. Catalytic roles for Ser-328 and Glu-470 appear more obvious. Amino acid 328 is located at the hinge of loop 6 that closes over the catalytic site to facilitate intra-molecular interactions that influences both the fixation rate and partiality for carboxylation or oxygenation[40]. Loop 6 closure involves the L-subunit C-terminus where amino acid 470 resides (Fig 5b). As a hydrophobic Ala-470 in the Paniacea NAD-ME and C_3 Rubisco, burial of the side chains into the enzyme surface may slow C-terminus movement. In contrast, Glu/Gln-470 might enhance solvent exposure and increase C-terminal tail mobility to alter the dynamics of loop 6 closure and stimulate k_{cat}^{c}.

We sought to test the possible role of L-subunit amino acid replacement(s) in influencing the variability in kinetics and temperature response among Paniceae Rubisco by tobacco chloroplast transformation. Multiple chloroplast genome (plastome) transformed tobacco lines were made (tob^{PdL} and tob^{PbL}) where the tobacco plastome *rbc*L gene was replaced with the *rbc*L gene from *P. bisulcatum* or *P. deustum* were generated (Fig S7a). Each transformed line was unable to survive outside of tissue culture (Fig 5c). Despite producing ample levels of *Panicum rbc*L mRNA (Fig S7b), no hybrid L_8S_8 holoenzyme (comprising *Panicum* L-subunits and tobacco S-subunits, Fig S7c) or unassembled *Panicum* L-subunits (Fig S7d) were detected. This suggests there are incompatibilities in the biogenesis requirements (translation, folding and/or assembly) of Rubisco between monocot and dicot species.

Discussion:

As calls for expanding the range of Rubiscos included in catalytic diversity studies increase, so should the range of temperatures examined. Unlike prior C_3-focused Rubisco diversity studies, our high resolution catalytic screen revealed variation in the kinetic trajectories of Paniceae Rubisco capable of enhancing C_3-photosynthesis at temperatures otherwise missed, or misjudged, from assaying at 25°C and one or two other temperatures.

Our analyses validate the co-evolution of higher k_{cat}^{c} and K_C across C_4-Rubiscos in response to a CCM[4,8,12,16,18,20], and unveil the widest variability in temperature kinetics reported for vascular plant Rubisco to date. We uniquely reveal alignment of Rubisco kinetics with CCM biochemistry and Paniceae biogeography. For example, the higher k_{cat}^{c} and K_C of the NADP-ME and PCK Paniceae Rubisco correlated with the forecast higher BSC CO_2 levels in these C_4-subtypes relative to the NAD-ME and the CCM deficient C_3/C_2 species[41]. The slower decline in $S_{C/O}$ by PCK and NADP-ME Rubisco under increasing temperature (Fig 3e) may reflect their warmer origins relative to the drier and cooler origins of NAD-ME and C_3 grasses, respectively[42]. Endeavors to determine whether these correlations extend to other C_4-species should take heed of inaccurately extrapolating the response of k_{cat}^{c} to temperature using a single Arrhenius fit rather than correctly accounting for its biphasic response that deviates at ~25°C (Fig 3b) – a relationship recognized 40 years ago[32], but whose mechanistic origin remains an unsolved.

The clustering of carboxylase properties of Paniceae Rubisco according to photosynthetic physiology contrasted with the more variable oxygenase activities (Fig 1i & j) supporting assertions these competing reactions can evolve independently due to differences in the mechanism and energy profile of their multi-step reactions[23]. This variability engenders natural kinetic diversity which, on the Rubisco superfamily scale, is relatively restricted for C_3-Rubisco[2,14,17,21,25,29 19,31]. In contrast the broad kinetic diversity among Paniceae Rubisco presents opportunities for enhancing C_3-photosynthesis under varying atmospheric CO_2 and temperature (Fig S5). In particular *P. bisulcatum* (C_3) and *P. deustum* (PCK) Rubisco could distinctly improve C_3-photosynthetic potential under cooler and warmer temperatures, respectively, relative to the standardized tobacco Rubisco control (Fig 4) #wheat/rice. The simulated improvements stemmed from temperature dependent enhancements in $S_{C/O}$ and/or k_{cat}^{c} / $K_{C}^{21\%O2}$ (Fig. 3d,e), and not necessarily from high k_{cat}^{c} (as emphasized by[8]). Our findings suggest that improving C_3-crop photosynthesis under warmer future climates may be best served by exploring the Rubisco kinetic diversity of C_4-land plants, in particular among PCK and NADP-ME species.

Four L-subunit residues could contribute kinetic diversity among Paniceae Rubisco. These included two amino acids within structural regions whose movements influence Rubisco kinetics: the catalytic loop 6 (residue 328) and C-terminal tail (residue 470). Positive selection of Ala-328-Ser substitutions have been reported for some *Limonium* haplotypes[43] and a few C_3 and CAM plant species[17]. This suggests the higher k_{cat}^{c} and K_C of Paniceae NADP-ME and PCK Rubisco might arise from the Glu/Gln-470 substitution (Fig 5a). Our attempts to test this by heterologous expression in tobacco chloroplasts proved unsuccessful (Fig 5c). The transformation limitation appears associated with differences in the ancillary protein requirements of Paniceae Rubisco biogenesis (Fig 5C), a constraint also preventing the production of Rubisco from red algae[44] and seemingly other monocot species[45] in tobacco chloroplasts.

Our data indicate the S-subunits also likely influence the kinetic diversity among Paniceae Rubisco. A comparable kinetic determining property was postulated for S-subunits in rice and wheat Rubisco[34,35]. In *P. virgatum* four *RbcS* mRNAs are made (Phytozome) whose translated 121-123 amino acid S-subunits vary by 1 to 6 residues. Mutagenic study of the multiple *Rbc*S transcripts produced in Paniceae would be a significant undertaking, but one possibly made easier using modern site specific nucleus gene editing tools that are now available in a variety of crop species[46]. Clarifying the influence of S-subunits on the temperature kinetics of Rubisco from differing plant origins is critical to developing appropriate L- and/or S-subunit mutagenic technologies for modifying crop Rubisco kinetics to suit future climates.

Corresponding author for material requests is spencer.whitney@anu.eud.au

Acknowledgements

We thank Asaph Cousins for supplying their *S. viridis* Rubisco kinetic data for analysis. This research was funded by the following grants from the Australian Research Council: DE130101760 (RES), DP120101603 (OG, SMW) and CE140100015 (OG, SMW).

Author contributions

RS, OG and SMW designed the study and undertook the experimental work. MVK undertook the phylogenetic analysis and LHG the structural analysis. All authors contributed to drafting the paper.

Competing financial interests

The authors declare no competing financial interests.

References

1 Ort, D. R. *et al.* Redesigning photosynthesis to sustainably meet global food and bioenergy demand. *Proc Natl Acad Sci U S A* **112**, 8529-8536 (2015).

2 Zhu, X. G., Long, S. P. & Ort, D. R. Improving photosynthetic efficiency for greater yield. *Annu Rev Plant Biol* **61**, 235-261 (2010).

3 Long, Stephen P., Marshall-Colon, A. & Zhu, X.-G. Meeting the global food demand of the future by engineering crop photosynthesis and yield potential. *Cell* **161**, 56-66 (2015).

4 Carmo-Silva, E., Scales, J. C., Madgwick, P. J. & Parry, M. A. J. Optimizing Rubisco and its regulation for greater resource use efficiency. *Plant Cell Env* **38**, 1817-1832 (2015).

5 Evans, J. R. Improving photosynthesis. *Plant Physiol* **162**, 1780-1793 (2013).

6 Parry, M. A. J. *et al.* Rubisco activity and regulation as targets for crop improvement. *J Exp Bot* **64**, 717-730 (2013).

7 von Caemmerer, S., Quick, W. P. & Furbank, R. T. The development of C_4 rice: current progress and future challenges. *Science* **336**, 1671-1672 (2012).

8 Whitney, S. M., Houtz, R. L. & Alonso, H. Advancing our understanding and capacity to engineer nature's CO_2-sequestering enzyme, Rubisco. *Plant Physiol* **155**, 27-35 (2011).

9 Andersson, I. Catalysis and regulation in Rubisco. *J Exp Bot* **59**, 1555-1568 (2008).

10 Andersson, I. & Backlund, A. Structure and function of Rubisco. *Plant Physiol Biochem* **46**, 275-291 (2008).

11 Sharwood, R. E., Ghannoum, O. & Whitney, S. M. Prospects for improving CO_2 fixation in C_3-crops through understanding C_4-Rubisco biogenesis and catalytic diversity. *Currt Opin Plant Biol* **31**, 135-142 (2016).

12 Carmo-Silva, A. E. *et al.* Rubisco activities, properties, and regulation in three different C_4 grasses under drought. *J Exp Bot* **61**, 2355-2366 (2010).

13 Galmes, J. *et al.* Expanding knowledge of the Rubisco kinetics variability in plant species: environmental and evolutionary trends. *Plant Cell Environ* **37**, 1989-2001 (2014).

14 Galmés, J., Kapralov, M. V., Copolovici, L. O., Hermida-Carrera, C. & Niinemets, Ü. Temperature responses of the Rubisco maximum carboxylase activity across domains of life: phylogenetic signals, trade-offs, and importance for carbon gain. *Photosynth Res* **123**, 183-201 (2015).

15 Jordan, D. B. & Ogren, W. L. The CO_2/O_2 specificity of ribulose 1,5-bisphosphate carboxylase oxygenase - dependence on ribulosebisphosphate concentration, pH and temperature. **161**, 308-313 (1984).

16 Prins, A. *et al.* Rubisco catalytic properties of wild and domesticated relatives provide scope for improving wheat photosynthesis. *J Exp Bot* **67**, 1827-1838 (2016).

17 Young, J. N. *et al.* Large variation in the Rubisco kinetics of diatoms reveals diversity among their carbon-concentrating mechanisms. *J Exp Bot* **67**, 3445-3456 (2016).

18 Andrews, T. J. & Whitney, S. M. Manipulating ribulose bisphosphate carboxylase/oxygenase in the chloroplasts of higher plants. *Arch.Biochem.Biophys.* **414**, 159-169 (2003).

19 Raven, J. A. Rubisco: still the most abundant protein of Earth? *New Phytol* **198**, 1-3 (2013).

20 Sage, R. F. The evolution of C_4 photosynthesis *New Phytol* **161**, 341-370 (2004).

21 Sage, R. F., Christin, P.-A. & Edwards, E. J. The C_4 plant lineages of planet Earth. *J Exp Bot* **62**, 3155-3169 (2011).

22 Furbank, R. T. Evolution of the C_4 photosynthetic mechanism: are there really three C_4 acid decarboxylation types? *J Exp Bot* **62**, 3103-3108 (2011).

23 Sage, R. F., Sage, T. L. & Kocacinar, F. Photorespiration and the evolution of C_4 photosynthesis. *Ann Rev Plant Biol* **63**, 19-47 (2012).

24 Ghannoum, O. *et al.* Faster rubisco is the key to superior nitrogen-use efficiency in NADP-malic enzyme relative to NAD-malic enzyme C_4 grasses. *Plant Physiol* **137**, 638-650 (2005).

25 Sharwood, R., von Caemmerer, S., Maliga, P. & Whitney, S. The catalytic properties of hybrid Rubisco comprising tobacco small and sunflower large subunits mirror the kinetically equivalent source Rubiscos and can support tobacco growth. *Plant Physiol* **146**, 83-96 (2008).

26 Sharwood, R. E., Sonawane, B. V., Ghannoum, O. & Whitney, S. M. Improved analysis of C_4 and C_3 photosynthesis via refined in vitro assays of their carbon fixation biochemistry. *J Exp Bot* **67**, 3137-3148 (2016).

27 Whitney, S. M. & Sharwood, R. E. Construction of a tobacco master line to improve Rubisco engineering in chloroplasts. *J Exp Bot* **59**, 1909-1921 (2008).

28 Tcherkez, G. G. B., Farquhar, G. D. & Andrews, T. J. Despite slow catalysis and confused substrate specificity, all ribulose bisphosphate carboxylases may be nearly perfectly optimized. *Proc Nat Acad Sci* **103**, 7246-7251 (2006).

29 Boyd, R. A., Gandin, A. & Cousins, A. B. Temperature response of C_4 photosynthesis: biochemical analysis of Rubisco, phosphoenolpyruvate carboxylase and carbonic anhydrase in *Setaria viridis*. *Plant Physiol* **169**, 1850-1861 (2015).

30 Perdomo, J. A., Cavanagh, A. P., Kubien, D. S. & Galmés, J. Temperature dependence of in vitro Rubisco kinetics in species of *Flaveria* with different photosynthetic mechanisms. *Photosynth Res* **124**, 67-75 (2015).

31 Sage, R. F. Variation in the k_{cat} of Rubisco in C_3 and C_4 plants and some implications for photosynthetic performance at high and low temperature. *J Exp Bot* **53**, 609-620 (2002).

32 Savir, Y., Noor, E., Milo, R. & Tlusty, T. Cross-species analysis traces adaptation of Rubisco toward optimality in a low-dimensional landscape. *Proc Nat Acad Sci* **107**, 3475-3480 (2010).

33 Pearcy, R. W. & Ehleringer, J. Comparative ecophysiology of C_3 and C_4 plants. *Plant Cell Env* **7**, 1-13 (1984).

34 Tcherkez, G. The mechanism of Rubisco-catalyzed oxygenation. *Plant Cell Env* **39**, 983-997 (2016).

35 Farquhar, G. D., von Caemmerer, S. & Berry, J. A. A biochemical model of photosynthetic CO_2 assimilation in leaves of C_3 species. *Planta* **149**, 78-90 (1980).

36 Sharwood, R. E. & Whitney, S. M. Correlating Rubisco catalytic and sequence diversity within C_3 plants with changes in atmospheric CO_2 concentrations. *Plant Cell Env* **37**, 1981-1984 (2014).

37 Sharkey, T. D., Bernacchi, C. J., Farquhar, G. D. & Singsaas, E. L. Fitting photosynthetic carbon dioxide response curves for C_3 leaves. *Plant Cell Env* **30**, 1035-1040 (2007).

38 Walker, B., Ariza, L. S., Kaines, S., Badger, M. R. & Cousins, A. B. Temperature response of *in vivo* Rubisco kinetics and mesophyll conductance in *Arabidopsis thaliana*: comparisons to *Nicotiana tabacum*. *Plant Cell Env* **36**, 2108-2119 (2013).

39 Hermida-Carrera, C., Kapralov, M. V. & Galmés, J. Rubisco catalytic properties and temperature response in crops. *Plant Physiol.*, doi:10.1104/pp.16.01846 (2016).

40 Orr, D. *et al.* Surveying Rubisco diversity and temperature response to improve crop photosynthetic efficiency. *Plant Physiol.*, doi:10.1104/pp.16.00750 (2016).

41 Badger, M. R. & Collatz, G. J. Studies on the kinetic mechanism of RuBP carboxylase and oxygenase reactions, with particular reference to the effect of temperature on kinetic papameters. *Carnegie YB* **76**, 355-361 (1977).

42 Ishikawa, C., Hatanaka, T., Misoo, S., Miyake, C. & Fukayama, H. Functional incorporation of sorghum small subunit increases the catalytic turnover rate of Rubisco in transgenic rice *Plant Physiol* **156**, 1603-1611 (2011).

43 Hauser, T., Popilka, L., Hartl, F. U. & Hayer-Hartl, M. Role of auxiliary proteins in Rubisco biogenesis and function. *Nat Plants* **1** (2015).

44 Wachter, R. M. *et al.* Activation of interspecies-hybrid Rubisco enzymes to assess different models for the Rubisco-Rubisco activase interaction. *Photosynth Res* **117**, 557-566 (2013).

45 Spreitzer, R. J., Peddi, S. R. & Satagopan, S. Phylogenetic engineering at an interface between large and small subunits imparts land-plant kinetic properties to algal Rubisco. *Proc Natl Acad Sci* **102**, 17225-17230 (2005).

46 von Caemmerer, S. & Furbank, R. T. The C_4 pathway: an efficient CO_2 pump. *Photosynth Res* **77**, 191-207, doi:10.1023/a:1025830019591 (2003).

47 Still, C. J., Pau, S. & Edwards, E. J. Land surface skin temperature captures thermal environments of C_3 and C_4 grasses. *Glob Ecol Biogeo* **23**, 286-296 (2014).

48 Galmés, J. *et al.* Environmentally driven evolution of Rubisco and improved photosynthesis and growth within the C_3 genus *Limonium* (Plumbaginaceae). *New Phytol* **203**, 989-999 (2014).

49 Whitney, S. M. & Andrews, T. J. Plastome-encoded bacterial ribulose-1, 5-bisphosphate carboxylase/oxygenase (RubisCO) supports photosynthesis and growth in tobacco. *Proc Nat Acad Sci* **98**, 14738-14743 (2001).

50 Bortesi, L. & Fischer, R. The CRISPR/Cas9 system for plant genome editing and beyond. *Biotech Adv* **33**, 41-52 (2015).

Figure Legends

Figure 1

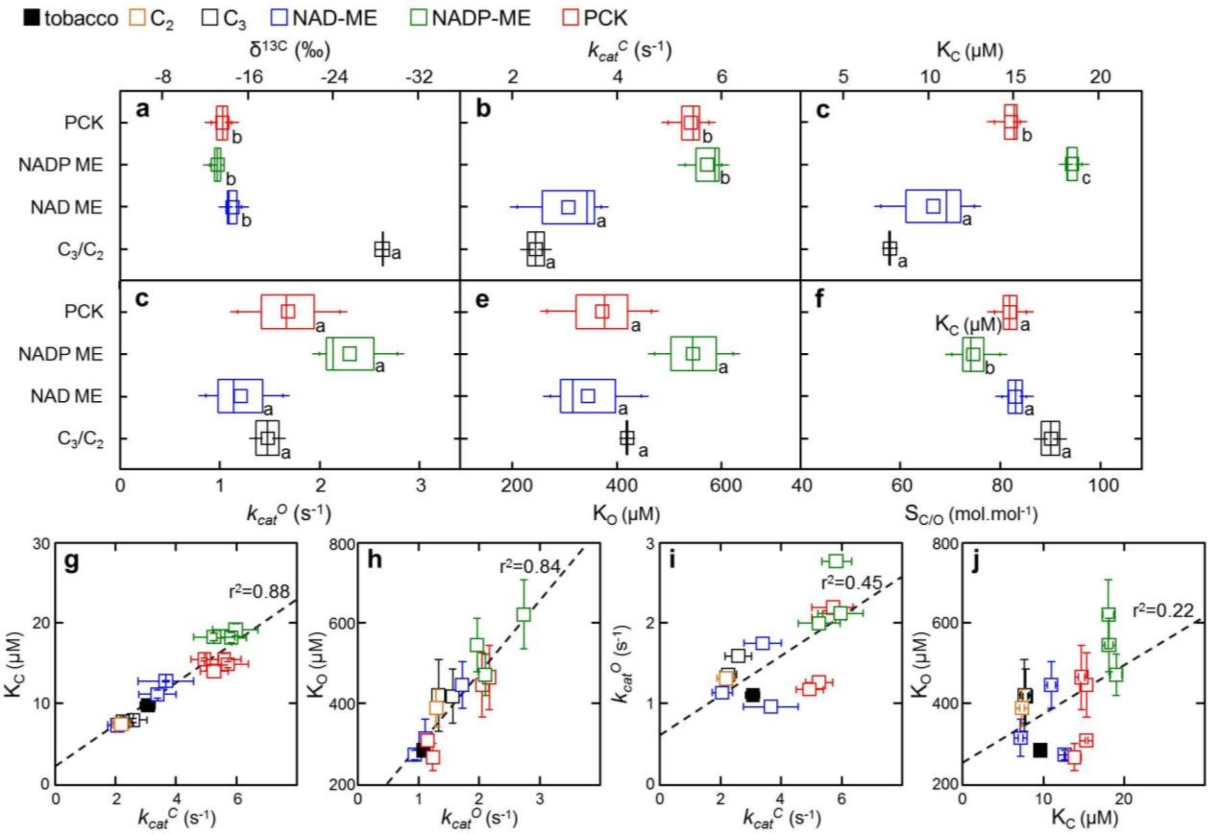

Figure 1. The diversity in the catalytic properties of Rubisco at 25°C across C_3 and C_4 grasses within Paniceae.

Box plots of comparative (**a**) leaf dry matter $^{12}C/^{13}C$ isotopic fractionation (δ^{13C}) and (**b** to **f**) *in vitro* measured Rubisco kinetics from tobacco and Paniceae species with C_2, C_3 and varying C_4 subtypes (NADP ME, NAD ME and PCK). See Table S1 for species list. Median values shown in boxes as vertical line, 95% confidence limits represented by horizontal lines. Letter variation indicates significant differences ($p < 0.05$) between parameters (Table S1). Kinetic properties analyzed include (**b**) substrate saturated carboxylation and (**d**) oxygenation turnover rates (k_{cat}^{c}, k_{cat}^{o}), the Michaelis constants (K_m) for (**c**) CO_2 and (**e**) O_2 (K_C, K_O) and (**f**) relative specificity for CO_2 over O_2 ($S_{C/O}$). (**g** to **j**) Pairwise relationships among the kinetic parameters to assess the quality of their linear correlations (dashed line).

Figure 2

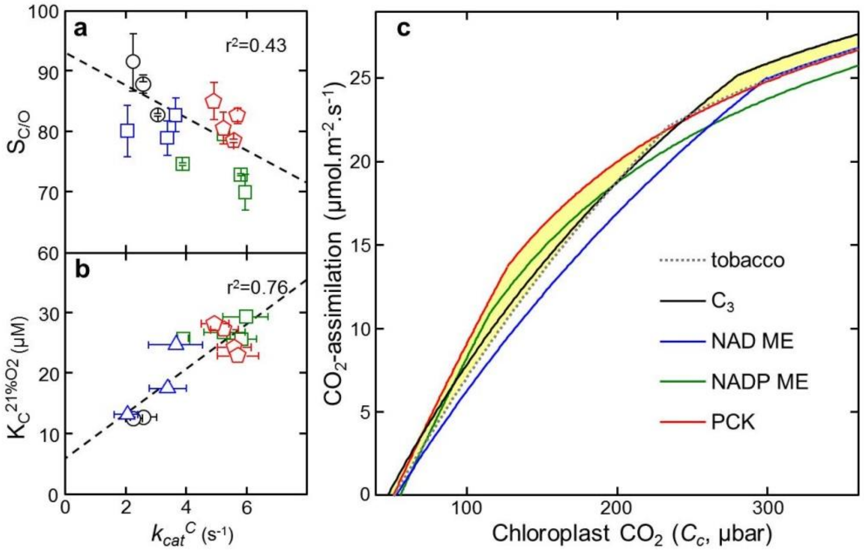

Figure 2. Variation among the Paniceae Rubisco kinetics differentially affect simulated rates of C_3-photosynthesis at 25°C.

Comparison of the relationships between k_{cat}^{c} and either (**a**) $S_{C/O}$ or (**b**) $K_C^{21\%O2}$, the value for Kc under ambient O_2 (O) calculated as $K_C(1+O/K_O)$ (Table S1). The r^2 values show the quality of their linear correlations (dashed lines). (**c**) The influence of the averaged Paniceae C_3 and C_4 subtype Rubisco kinetics (Table S1) on CO_2 assimilation rates (A) at 25°C in a C_3-leaf as a function of C_c. Lines are modelled (Farquhar et al., (1980)) using the carboxylase activity limited assimilation equation:

$$A = \frac{(C_c.s_c - 0.5\ O/S_{c/o})\ \ k_{cat}{}^{c}\ .B}{C_c.s_c + K(1 + O/Ko)} - R_d$$

using a CO_2 solubility in H_2O (s_c) of 0.0334M bar^{-1}, an *O* of 253 µM, a Rubisco content (*B*) of 30 µmol catalytic sites.m^{2} and a non-photorespiratory CO_2 assimilation rate (R_d) of 1 µmol.m^{-2}.s^{-1}. The light limited CO_2 assimilation rates (to the right of the symbols) were modelled according to the equation:

$$A = \frac{(C_c.s_c - 0.5\ O/S_{c/o})\ J}{4(C_c.s_c + O/S_{c/o})} - R_d$$

assuming an electron transport rate (*J*) of 160 µmol.m^{-2}.s^{-1}. Yellow shading indicates where the modeled CO_2-assimilation rates of C_3, NADP-ME and PCK Paniceae Rubisco exceed that of Rubisco from the model C_3-plant, tobacco (dotted line).

Figure 3

a

Rubisco grouping	# of species	k_{cat}^{C} (< 25°C)		k_{cat}^{C} (> 25°C)		$K_C^{21\%O2}$		$S_{C/O}$	
		ΔH_a (±S.E.) (kJ mol^{-1})	*c* (±S.E.)	ΔH_a (±S.E.) (kJ mol^{-1})	*c* (±S.E.)	ΔH_a (±S.E.) (kJ mol^{-1})	*c* (±S.E.)	ΔH_a (±S.E.) (kJ mol^{-1})	*c* (±S.E.)
tobacco	n=1	60.3	25.5	36.4	15.8	37.3	17.9	22.5	-4.7
C_3/C_2	n=2	69.8 ± 1.4^{b}	29.0 ± 0.6^{b}	36.3 ± 4.0^{b}	15.5 ± 1.5^{b}	28.2 ± 2.8^{a}	13.9 ± 1.1^{a}	28.6 ± 1.1^{b}	-7.1 ± 0.4^{a}
NAD ME	n=3	62.7 ± 4.5^{ab}	26.4 ± 1.6^{a}	27.6 ± 2.3^{ab}	12.2 ± 0.9^{a}	30.0 ± 4.4^{a}	15.0 ± 1.8^{a}	25.3 ± 1.6^{ab}	-5.8 ± 0.7^{ab}
NADP ME	n=3	56.0 ± 0.6^{a}	24.4 ± 0.2^{a}	27.7 ± 1.4^{a}	12.9 ± 0.5^{a}	25.8 ± 4.0^{a}	13.7 ± 1.6^{a}	22.8 ± 2.0^{a}	-5.0 ± 0.8^{b}
PCK	n=3	55.6 ± 2.8^{a}	24.1 ± 1.1^{a}	26.4 ± 1.0^{a}	12.3 ± 0.4^{a}	26.9 ± 2.4^{a}	14.1 ± 0.9^{a}	21.8 ± 0.5^{a}	-4.4 ± 0.2^{b}

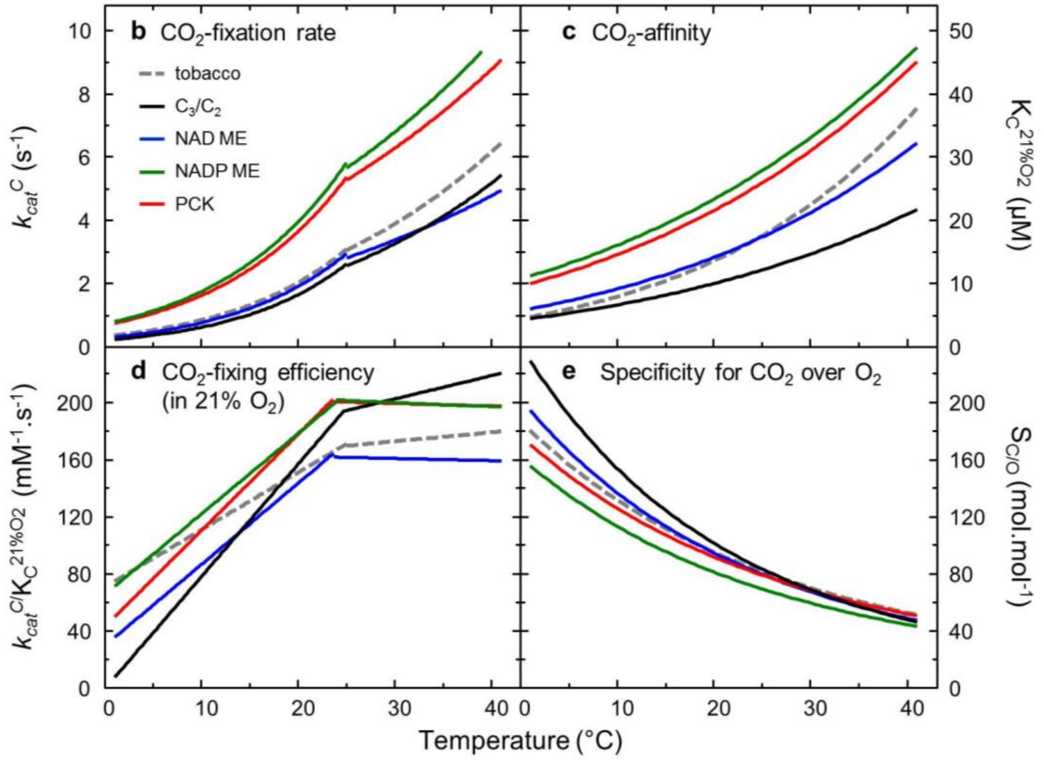

Figure 3. Divergence in the catalytic properties of Paniceae and tobacco Rubisco in response to temperature.

(**a**) The heat of activation (ΔH_a) and scaling constant (*c*) for the kinetic parameters of tobacco Rubisco and the mean (±S.E) values measured for the various Paniceae species with C_4 (NAD ME, NADP ME, PCK) or C_3 (including the aligning C_2) biochemical physiologies (see Table S3). Letters show the statistical ranking using a post hoc Tukey test among the biochemical physiology groupings (different letters indicated differences at the 5% level, $p < 0.05$). (**b** to **e**) Differences in the temperature response of tobacco (grey dashed line) and the averaged kinetic properties for Rubisco from Paniceae species with varying biochemical physiologies. The lines are derived as described in Figures S1 to S4 using the values listed in panel (**a**).

Figure 4

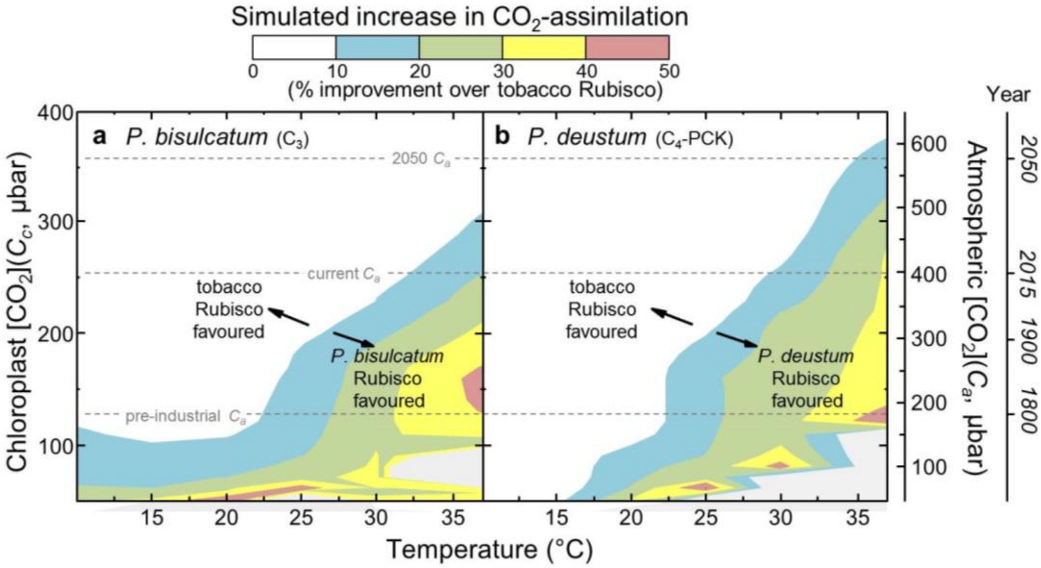

Figure 4. The potential for improving the thermal response of C_3-photosynthesis.

The benefits of (**a**) *P. bisulcatum* (C_3) and (**b**) *P. deustum* (C_4-PCK) Rubisco to the rate of photosynthesis in a C_3-leaf under varying chloroplast CO_2 concentrations (C_a) and temperature (see scale). Rate increases are presented as a percentage above that provided by tobacco Rubisco. The data was modelled according to[24] using the parameters listed in Table S4 and plotted in Fig S4.

Figure 5

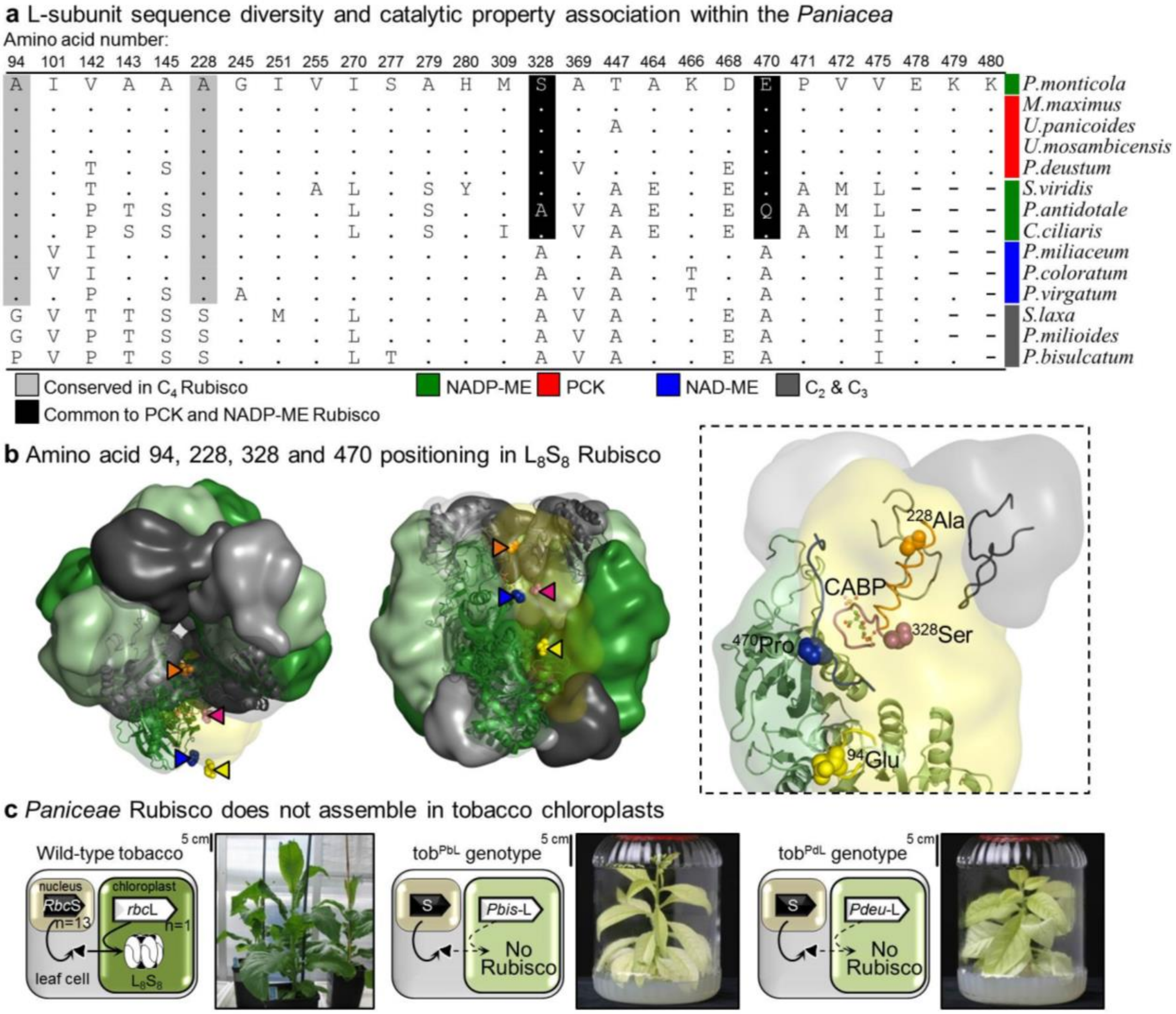

a L-subunit sequence diversity and catalytic property association within the *Paniacea*

Amino acid number:

94	101	142	143	145	228	245	251	255	270	277	279	280	309	328	369	447	464	466	468	470	471	472	475	478	479	480		
A	I	V	A	A	A	G	I	V	I	S	A	H	M	S	A	T	A	K	D	E	P	V	V	E	K	K	🟩	*P.monticola*
.	.	.	.	.	.	.	.	.	.	.	.	.	.	.	.	.	.	.	.	.	.	.	.	.	.	.	🟥	*M.maximus*
.	.	.	.	.	.	.	.	.	.	.	.	.	.	.	.	A	.	.	.	.	.	.	.	.	.	.	🟥	*U.panicoides*
.	.	.	.	.	.	.	.	.	.	.	.	.	.	.	.	.	.	.	.	.	.	.	.	.	.	.	🟥	*U.mosambicensis*
.	.	T	.	S	.	.	.	.	.	.	.	.	.	.	V	.	.	.	E	.	.	.	.	.	.	.	🟥	*P.deustum*
.	.	T	.	.	.	.	.	A	L	.	S	Y	.	.	.	A	E	.	E	.	A	M	L	–	–	–	🟩	*S.viridis*
.	.	P	T	S	.	.	.	.	L	.	S	.	.	A	V	A	E	.	E	Q	A	M	L	–	–	–	🟩	*P.antidotale*
.	.	P	S	S	.	.	.	.	L	.	S	.	I	.	V	A	E	.	E	.	A	M	L	–	–	–	🟩	*C.ciliaris*
.	V	I	.	.	.	.	.	.	.	.	.	.	.	A	.	A	.	.	.	A	.	.	I	.	–	–	🟦	*P.miliaceum*
.	V	I	.	.	.	.	.	.	.	.	.	.	.	A	.	A	.	T	.	A	.	.	I	.	–	–	🟦	*P.coloratum*
.	.	P	.	S	.	A	.	.	.	.	.	.	.	A	V	A	.	T	.	A	.	.	I	.	.	–	🟦	*P.virgatum*
G	V	T	T	S	S	.	M	.	L	.	.	.	.	A	V	A	.	.	E	A	.	.	I	.	–	–	⬛	*S.laxa*
G	V	P	T	S	S	.	.	.	L	.	.	.	.	A	V	A	.	.	E	A	.	.	I	.	–	–	⬛	*P.milioides*
P	V	P	T	S	S	.	.	.	L	T	.	.	.	A	V	A	.	.	E	A	.	.	I	.	.	–	⬛	*P.bisulcatum*

▨ Conserved in C_4 Rubisco
■ Common to PCK and NADP-ME Rubisco
🟩 NADP-ME
🟥 PCK
🟦 NAD-ME
⬛ C_2 & C_3

b Amino acid 94, 228, 328 and 470 positioning in L_8S_8 Rubisco

c *Paniceae* Rubisco does not assemble in tobacco chloroplasts

Figure 5. Approaches to decipher possible catalytic switches in the L-subunit of Paniceae Rubisco.

(**a**) Amino acid variation in the L-subunit of each Paniacea Rubisco analysed in this study. A phylogenetic analysis of the L-subunit sequences and their Genbank accession information is provided in Figure S6. (**b**) Structure of spinach L_8S_8 Rubisco (L-subunits in green, S-subunits grey) viewed from the top (left) and side (middle) showing the relative locations of ^{94}Glu on the solvent-exposed Rubisco surface (yellow triangle), ^{228}Ala in the α2 helix (orange triangle), ^{328}Ser at the hinge of loop 6 (purple triangle) and ^{470}Pro in the C-terminal tail extension (blue triangle) of one L-subunit. A closer view of a L-subunit pair (right) with one showing ribbon structural detail and the other showing the positioning of ^{94}Glu, ^{228}Ala, ^{328}Ser and ^{470}Pro relative to each other, an N-terminal domain loop, the α2 helix, loop 6, C-terminal tail extension and S-subunit βA-βB loops (yellow, orange, purple, blue and grey, respectively). An active site bound reaction-intermediate analogue 2-CABP is shown as a ball and stick. (**c**) Chloroplast transformation of the Rubisco L-subunit genes from *P. bisulcatum* (*Pbis-rbc*L) and *P. deustum* (*Pbis-rbc*L) into tobacco was undertaken to identify the amino acids (catalytic switches) responsible for their differing catalytic properties. No Rubisco biogenesis was detected in the tob^{PbL} and tob^{PdL} tobacco genotypes produced. Accordingly these plants could only grow in tissue culture on sucrose containing media and were highly chlorotic (as shown). Detailed analysis of the transformation, Rubisco mRNA and protein biochemistry is provided in Figure S7.

Supplemental data

Variation in response of C_3 and C_4 Paniceae Rubisco to temperature provides opportunities for improving C_3 photosynthesis

Robert E. Sharwood[1+], Oula Ghannoum[2+]*, Maxim V. Kapralov[1,3], Laura H. Gunn[1,4], and Spencer M. Whitney[1+]*.

[1]Research School of Biology, Australian National University, Canberra ACT, 2601, Australia.

[2] Hawkesbury Institute for the Environment, Western Sydney University, Richmond NSW, 2753, Australia.

[+] ARC Centre of Excellence for Translational Photosynthesis, Australian National University Canberra ACT, 2601, Australia.

[3]Current Address: School of Natural Sciences and Psychology, Liverpool John Moores University, Liverpool, L3 3AF, United Kingdom.

[4]Current address: Department of Cell and Molecular Biology, Uppsala University, Uppsala, SE-751 24, Sweden.

*Corresponding Authors: o.ghannoum@westernsydney.edu.au and spencer.whitney@anu.eud.au

Number of Supplemental Figures: 7

Number of Supplemental Tables: 4

Supplementary Figure S1

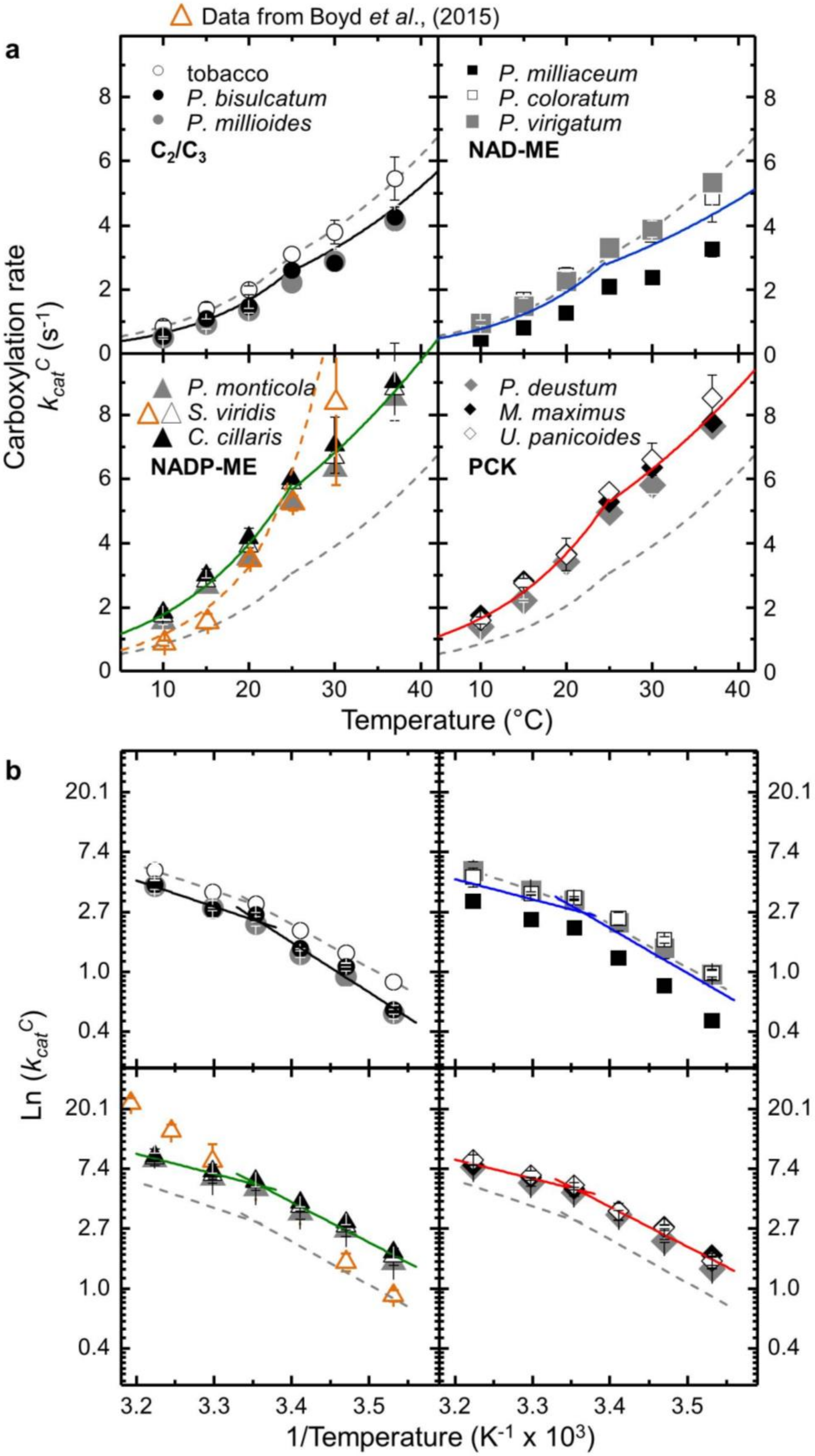

633

Figure S1. Variation in the temperature response of k_{cat}^{c} among the Paniceae and tobacco Rubisco.

(**a**) Substrate saturated rates of carboxylation (k_{cat}^{c}) determined using soluble leaf protein extract ($n \geq 3$ biological samples per species) were measured at 10, 15, 20, 25, 30 and 37°C with the expected exponential decrease in k_{cat}^{c} less evident at the lower assay temperatures for all Rubisco samples, as evident in prior published data [18-20,28,30-32] }, including that of Boyd et al., (2015) [15] (orange triangles) for *Seteria viridis* Rubisco measured by Membrane Inlet Mass Spectrometry (MIMS). Plotted data are listed in Table S2. (**b**) Evaluation of the data via Arrhenius-style plots (*i.e.* ln k_{cat}^{c} vs 1/T) indicated the k_{cat}^{c} response diverged at around 25°C. Shown are the averaged linear fits to each Arrhenius plot in a biphasic manner with the < 25°C measurements (*i.e.* at 10, 15, 20, 25°C) separated from the > 25°C measurements (25, 30 and 37°C). The averaged data values were fitted to the following equation

$$Parameter = exp\left[c - \frac{\Delta H_a}{RT}\right]$$

and the heat of activation (ΔH_a) for k_{cat}^{c} at both < 25°C and > 25°C was derived from the slope ($\ln(k_{cat}^{c}) = -\Delta H_a/R$; where R is the molar gas constant, 8.314 J K^{-1} mol^{-1}) and the scaling constant (c) from the ordinal intercept. The calculated values are listed in Table S3 and were fitted to the above equation to derive the exponential curves in panel **a**. For comparison, the fitted lines for tobacco Rubisco k_{cat}^{c} data are shown as dotted lines in each C_4 Rubisco plot. See Table S3 for statistical analysis.

Supplementary Figure S2

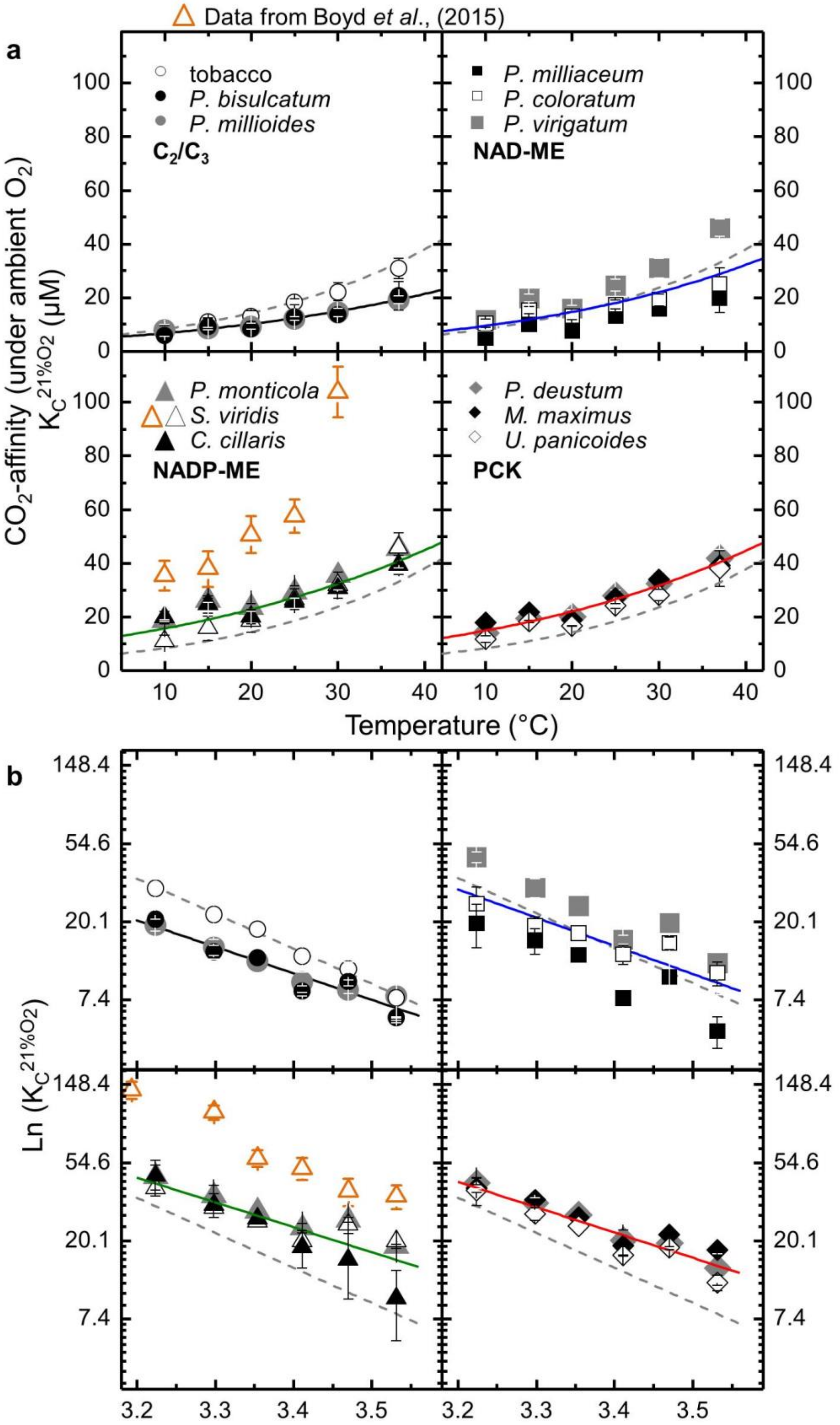

652

Figure S2. Variation in the temperature response of CO_2 affinity among the Paniceae and tobacco Rubisco.

(**a**) The Michealis constant for CO_2 measured in the presence of ambient (253 µM) O_2 concentration ($K_C^{21\%O2}$) determined from the same assays used to determine k_{cat}^c in Fig S1 ($n \geq 3$ biological samples analyzed per specie) varied exponentially over 10 to 37°C. Orange triangles, data for *Seteria viridis* Rubisco measured by MIMS[15]). Plotted data are listed in Table S2. (**b**) Arrhenius-style plots of the data with the averaged linear regression fitted as described in Fig S1 to determine the heat of activation (ΔH_a) and the scaling constant (*c*) values listed in Table S3 and used to derive the exponential curves shown in panel (**a**). As a scaling comparison, the fitted lines for tobacco Rubisco $K_C^{21\%O2}$ data are shown as dotted lines in each C_4 Rubisco plot. See Table S3 for statistical analysis.

Supplementary Figure S3

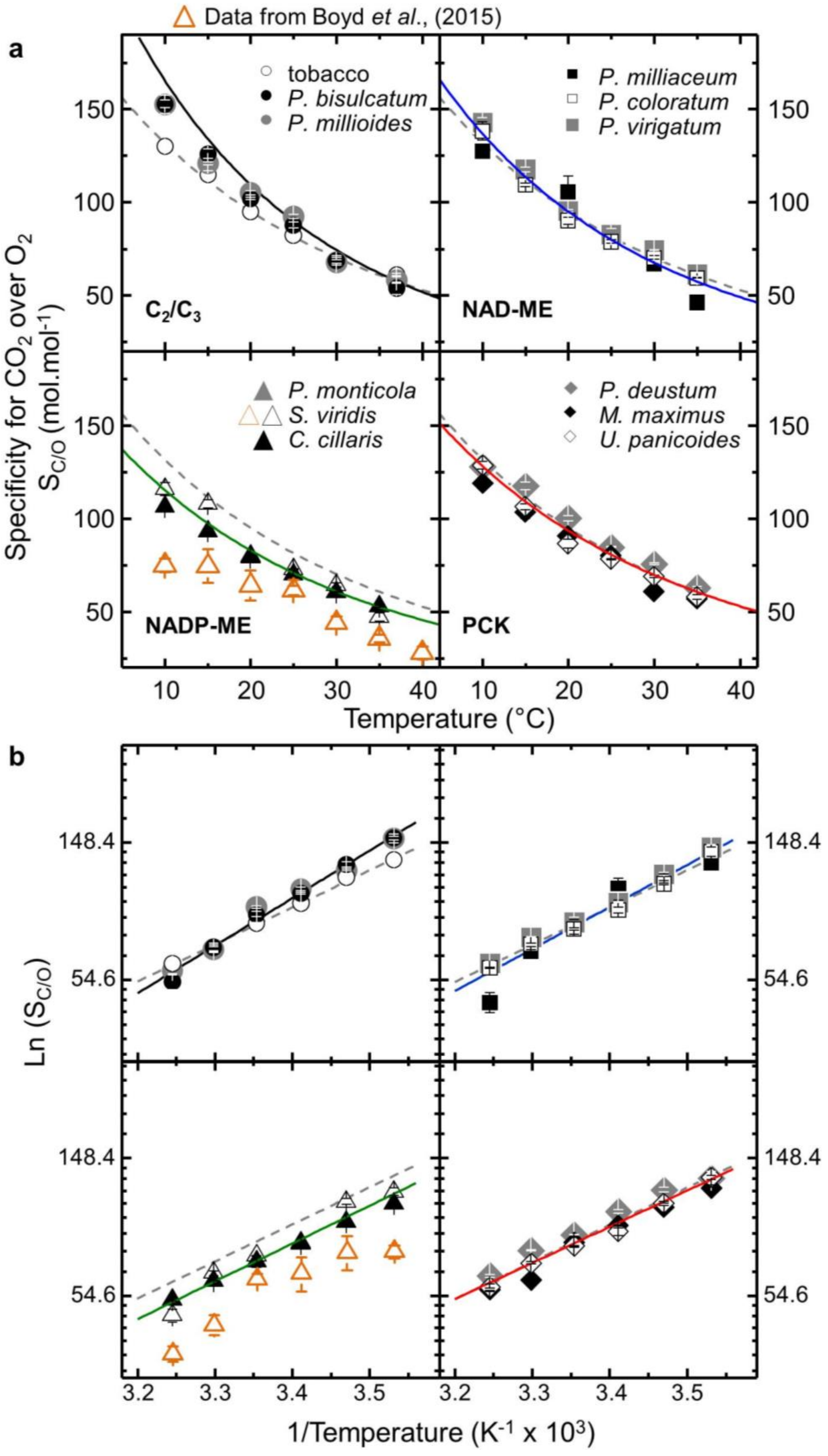

Figure S3. Variation in the temperature response of CO_2 over O_2 specificity among the Paniceae and tobacco Rubisco

(**a**) The influence of temperature on the specificity of CO_2 over O_2 ($S_{C/O}$) determined using Rubisco purified from at least two biological samples per specie. Orange triangles, data for *Seteria viridis* Rubisco measured by MIMS[15]. Plotted data are listed in Table S2. (**b**) Arrhenius plots of the data with the averaged linear regression fitted as described in Fig S1 to determine the heat of activation (ΔH_a) and the scaling constant (c) values for $S_{C/O}$ listed in Table S3 and used to derive the exponential curves shown in panel (**a**). The fitted lines for tobacco Rubisco $S_{C/O}$ data are shown as dotted lines in each C_4 Rubisco plot as a scaling comparison. See Table S3 for statistical analysis.

Supplementary Figure S4

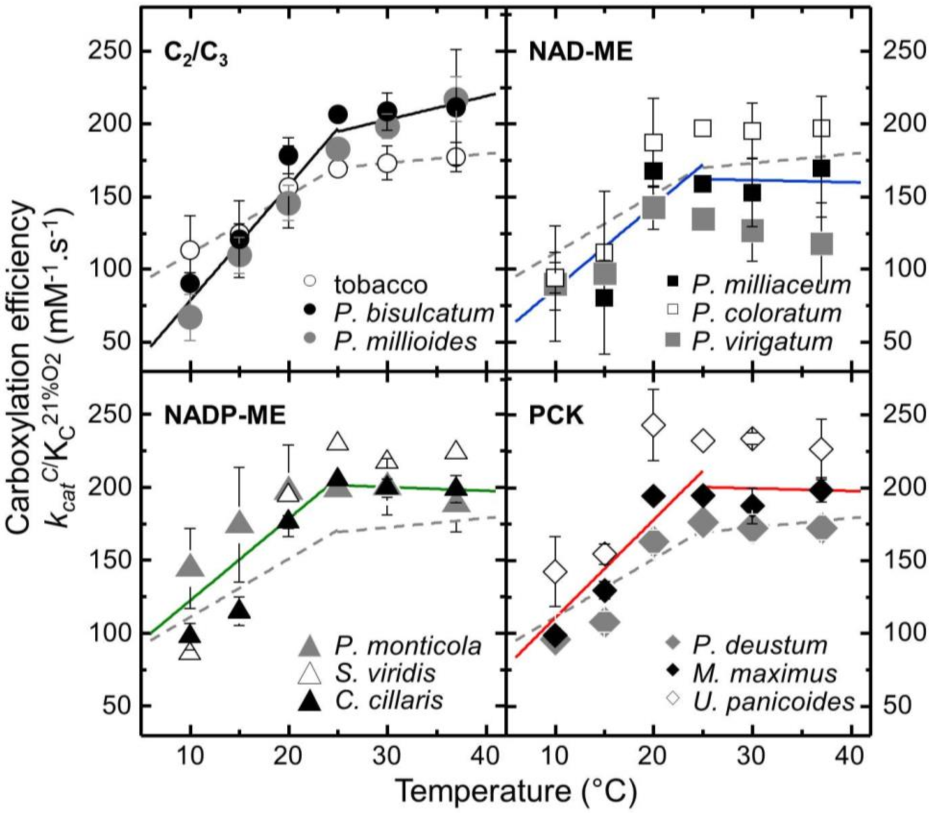

Figure S4. Variation in carboxylation efficiency under ambient O_2 among the Paniceae and tobacco Rubisco under varying temperature.

The temperature response of carboxylation efficiency ($k_{cat}^{c/}$ $K_C^{21\%O2}$) for each Rubisco was calculated by dividing the averaged values of k_{cat}^{c} (FigS1) by its corresponding $K_C^{21\%O2}$ values (Fig S2) for each assay temperature. As shown previously for *Flaveria* [19] and *Seteria viridis* [15] Rubisco, the carboxylation efficiency of each Paniceae and tobacco Rubisco declined at temperatures below 25°C and showed less variation at temperatures > 25°C. Shown are the linear regressions fitted to the averaged Paniceae data for each biochemical physiology. See Table S3 for statistical analysis.

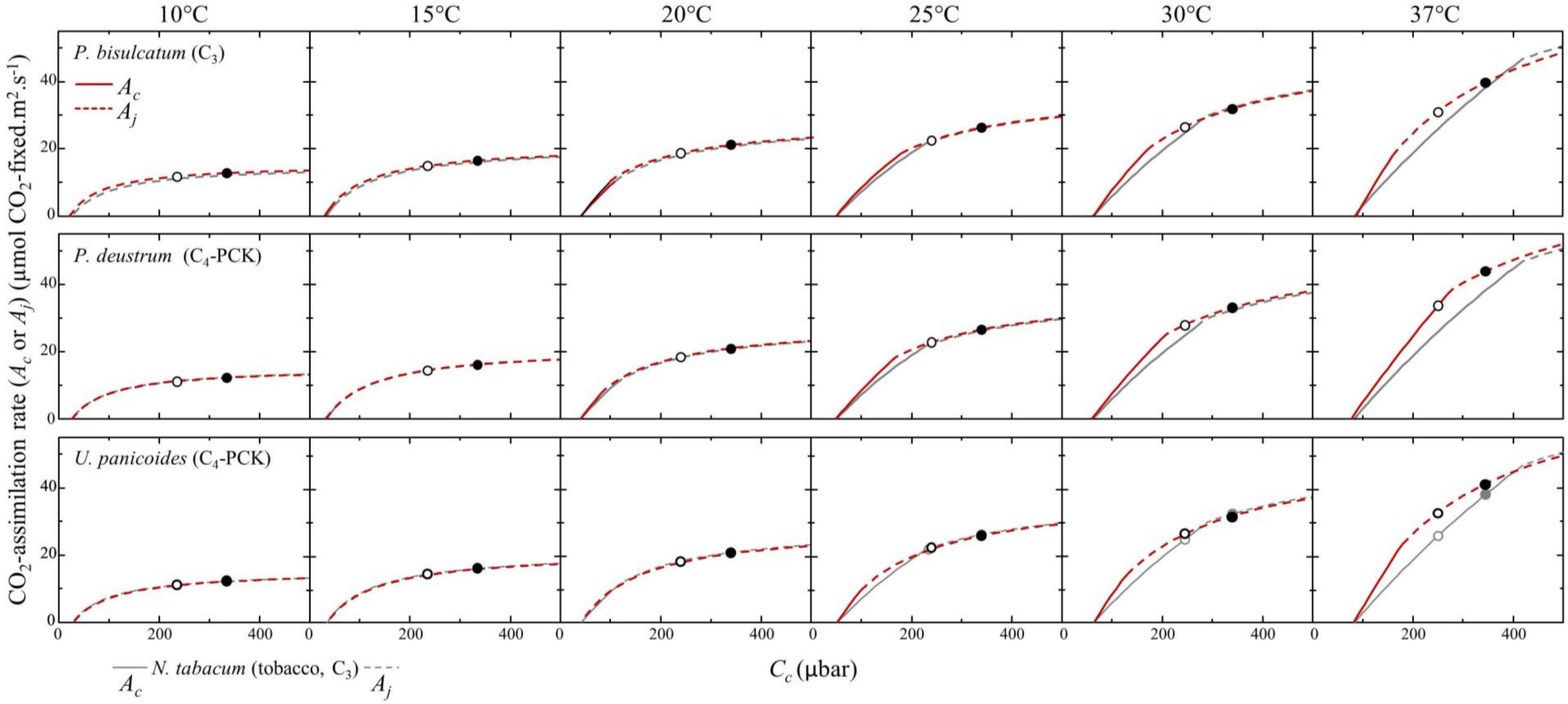

Figure S5. Effect of Rubisco kinetics on the thermal photosynthetic response.

The effects Rubisco catalytic properties on the thermal response of leaf photosynthesis (*A*) to leaf chloroplastic CO$_2$ concentration (C_c). The curves were modelled according to Farquhar *et al.* (1980) [24] using equations and parameters shown in Supplementary Table S5. The solid and dashed lines refer to the Rubisco limited (A_c) and RuBP-regeneration limited (A_j) assimilation rates, respectively. The circles refer to assimilation rates under current C_a (400 μbar, white) and that predicted for 2050 (550 μbar, black). Data for tobacco Rubisco shown in grey in each panel for comparison.

Supplementary Figure S6

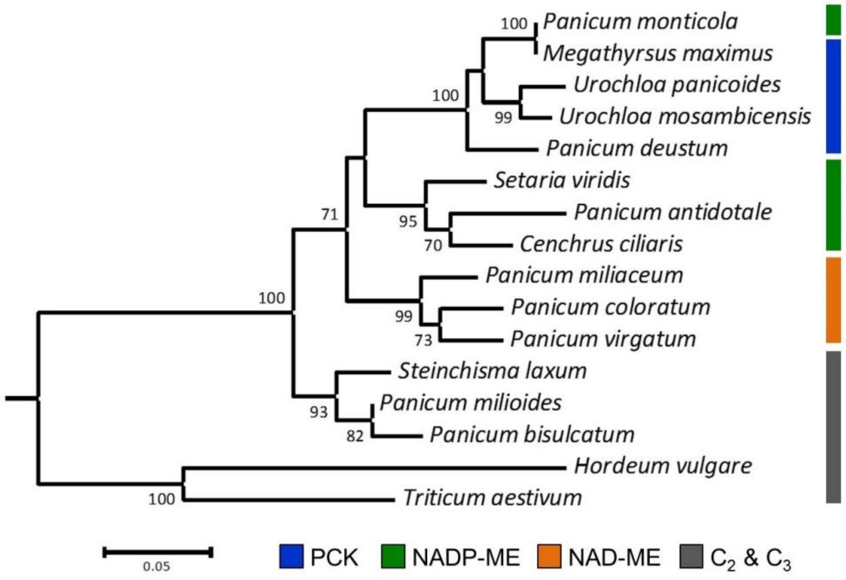

Figure S6. Rubisco L-subunit phylogeny in the Paniceae.

Maximum likelihood phylogeny of Rubisco L-subunit sequences from the fourteen Paniceae species examined in this study relative to the outgrouped Rubisco from *Hordeum vulgare* (barley) and *Triticum aestivum* (wheat). ML trees assembled under the Dayhoff model implemented in RAxML v.8 [47] using translated L-subunit sequences from the full length *rbc*L genes available from the following Genbank accession: *P. bisulcatum*, (*); *S. laxa*, (*); *P. milioides*, (*); *P. antidotale*, (*); *P. monticola*, (*); *C. ciliaris*, (*); *S. viridis*, (KT289405.1); *P. virgatum*, (HQ731441.1); *P. milliaceum* , (KU343177.1); *P. coloratum*, (*); *M. maximus*, (*); *U. panicoides*, (*); *U. panicoides* , (*); *P. deustum* , (*); *U. mosambicensis*, (*); *H. vulgare*, (KT962228.1) and *T. aestivum*, (KJ592713.1). *sequences submitted to Genbank, awaiting accession numbers.

Supplementary Figure S7

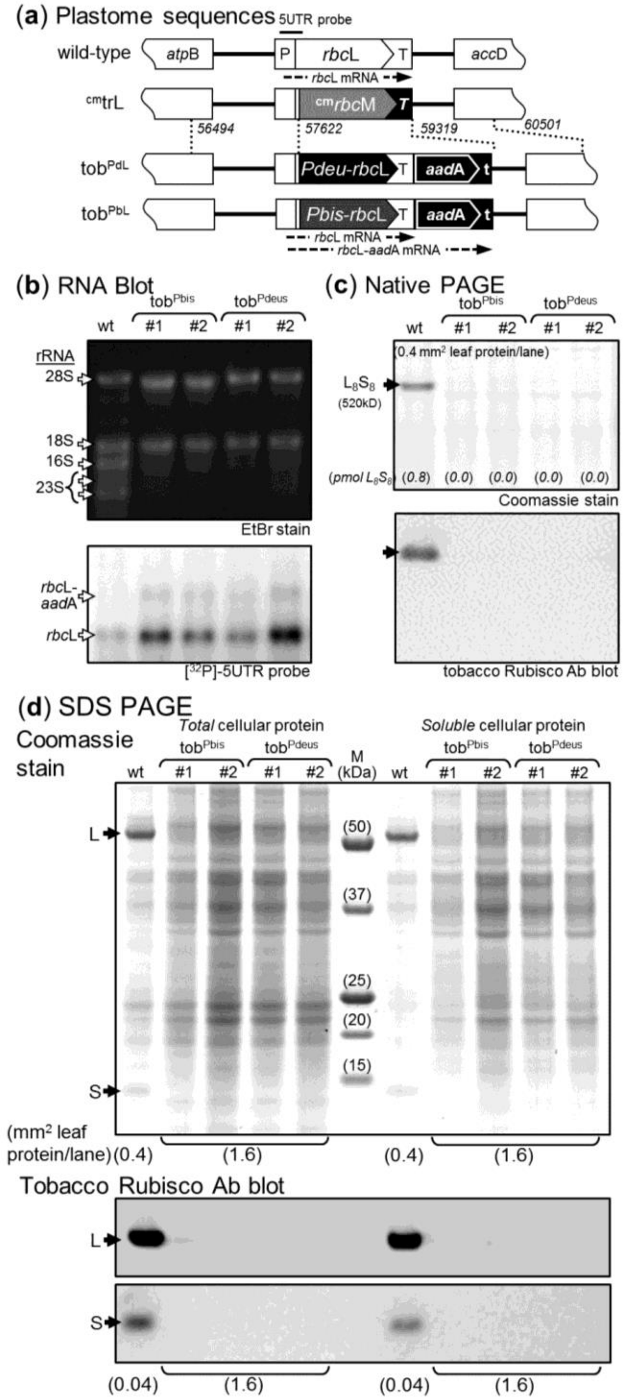

Figure S7. Chloroplast transformation of the *P. bisulcatum* (C_3) and *P. deustum* (C_4-PCK) *rbc*L genes to assess Paniceae Rubisco biogenesis in tobacco.

(**a**) Comparison of the plastome sequence in wild-type, ^{cm}trL and the plastome transformed tob^{PbL} and tob^{PdL} tobacco genotypes generated in this study. Duplicate tob^{PbL} and tob^{PdL} lines were made by plastome transformation as described [13] by homologous recombination replacement of the ^{cm}*rbc*M gene in the plastome of the ^{cm}trL tobacco genotype with *rbc*L genes for *P. bisulcatum* or *P. deustum* Rubisco (synthesized to match the tobacco *rbc*L nucleotide sequence where feasible) and the *aad*A selectable marker gene (coding resistance to spectinomycin). Numbering represents the flanking plastome sequence in the pLEVPdL and pLEVPbL transforming plasmids. P, 292-bp *rbc*L promoter/5'UTR; T, 288-bp*rbc*L 3'UTR; *T*, 112-bp of *psb*A 3'UTR; t, 147-bp *rps*16 3'UTR. Position of the 221-bp 5UTR probe [13] and the corresponding *rbc*L and *rbc*L-*aad*A mRNAs (dashed lines) to which it hybridizes are indicated. (**b**) Total leaf RNA (5μg) extracted from tissue culture grown plant samples was separated on denaturing formaldehyde gels and the EtBr stained RNA visualised (upper panel) before blotting onto Hybond-N nitrocellulose membrane (GE healthcare) as described [11] and probed with the ^{32}P-labelled 5UTR probe (lower panel). The probe correctly hybridised to the wild-type tobacco *rbc*L mRNA and the *rbc*L and *rbc*L-*aad*A mRNA transcripts in each tob^{PbL} and tob^{PdL} line. (**c**) Soluble leaf protein from the same leaves analyzed in (**b**) was processed for measuring Rubisco levels by NdPAGE analysis and ^{14}C-CABP quantification as described [25]. While wildtype tobacco L_8S_8 Rubisco was readily detected by ^{14}C-CABP binding, Coomassie staining and by immunoblot analysis with an antibody to tobacco Rubisco following ndPAGE, these methods detected no hybrid L_8S_8 Rubisco biogenesis in the tob^{PbL} and tob^{PdL} genotypes (*i.e.* complexes comprising the introduce *Panicum* L-subunits and the endogenous, cytosol made tobacco S-subunits). (**d**) Further inspection of the soluble and total (comprising soluble + insoluble) leaf protein separated by SDS PAGE did not detect any Rubisco L-subunit (~50 kDa) or S-subunit (~14.5

kDa) in either cellular protein fraction of the tob^{PbL} or tob^{PdL} lines by Comassie staining or Rubisco antibody blot analysis. This indicated that even when grown in tissue culture the resource limitations confronting the photosynthetically deplete tob^{PbL} and tob^{PdL} lines precluded the synthesis and /or accumulation of *Panicum* sp. Rubisco L-subunits. Whether co-expressing their cognate SSu or/and Raf1 [48] can circumvent this biogenesis challenge remains to be tested.

Table S1: Summary of the catalytic parameters of Paniceae and tobacco Rubisco at 25°C.

	Species	Physiology	δ^{13C}	k_{cat}^{c}	K_C	$K_C^{21\%\ O2}$	k_{cat}^{o}	K_O	k_{cat}^{o}/K_O	$S_{C/O}$	$k_{cat}^{c}/K_C^{21\%O2}$	k_{cat}^{c}/K_C
			(‰)	(s^{-1})	(µM)	(µM)	(s^{-1})	(µM)	($mM^{-1}.s^{-1}$)	($mol.mol^{-1}$)	($mM.^{-1}.s^{-1}$)	($mM.^{-1}.s^{-1}$)
Paniceae species	*Panicum antidotale*	C_4 NADP-ME	-12..92	3.9 ± 0.2	n.m	25.2	n.m	n.m	n.m	74.5 ± 0.4	156	n.m
	Panicum monticola		-13.53	5.3 ± 0.7	18.2 ± 0.5	26.6	2.0	543 ± 67	3.7	79.4 ± 1.7	198	290
	Cenchrus ciliaris		-12.46	6.0 ± 0.8	19.0 ± 0.7	29.2	2.1	470 ± 52	4.5	69.9 ± 3.0	205	314
	Setaria viridis		-13.81	5.9 ± 0.5	18.1 ± 0.6	25.5	2.8	619 ± 86	4.4	72.7 ± 0.2	230	323
	Panicum virgatum	C_4 NAD-ME	-13.98	3.3 ± 0.9	12.7 ± 0.1	24.5	0.9	271 ± 12	3.1	82.6 ± 2.8	133	258
	Panicum milliaceum		-15.50	2.1 ± 0.3	7.2 ± 0.3	13.1	1.1	313 ± 46	3.6	79.9 ± 4.3	159	287
	Panicum coloratum		-14.20	3.4 ± 0.6	11.1 ± 0.5	17.3	1.6	445 ± 58	3.6	84.8 ± 2.8	197	308
	Megathyrsus maximus	C_4 PCK	-14.32	5.3 ± 0.5	13.9 ± 0.8	27.1	1.3	265 ± 34	4.7	80.3 ± 2.8	195	380
	Urochloa panicoides		-14.51	5.6 ± 0.6	15.4 ± 0.7	24.1	2.1	444 ± 80	4.6	78.3 ± 0.3	232	364
	Panicum deustum		-12.62	5.0 ± 0.5	15.4 ± 0.2	28.1	1.2	306 ± 16	3.8	84.8 ± 0.2	177	322
	Urochloa mosambicensis		-13.08	5.7 ± 0.7	14.8 ± 0.4	22.8	2.2	464 ± 79	4.7	82.5 ± 1.3	252	388
	Panicum milioides	C_2	-31.50	2.2 ± 0.3	7.4 ± 0.3	12.1	1.3	387 ± 46	3.3	92.3 ± 1.0	182	301
	Panicum bisulcatum	C_3	-28.68	2.6 ± 0.4	7.8 ± 0.3	12.6	1.6	416 ± 67	3.8	87.7 ± 1.5	207	333
	Steinchisma laxa		-28.70	2.3 ± 0.3	7.7 ± 0.5	12.4	1.4	419 ± 89	3.2	91.4 ± 4.8	184	294
Nicotiana tabacum			n.m.	3.1 ± 0.3	9.7 ± 0.1	18.3	1.1	283 ± 15	3.9	82.6 ± 0.8	168	318
Averages of parameters for Paniceae Rubisco		C_3	-28.7±0.1 a	2.4±0.2 a	7.8±0.1 a	12.5±0.1 a	1.5±0.1 a	418±1 a	3.5±0.3 a	90±2 a	195±12 a	313±19 ab
		NAD-ME	-14.6±0.5 b	2.9±0.4 a	10.3±1.6 a	18.3±3.3 a	1.2±0.2 a	343±52 a	3.4±0.2 a	82±1 a	163±18 a	284±15 a
		NADP-ME	-13.3±0.4 b	5.7±0.2 b	18.4±0.3 c	27.1±1.1 b	2.3±0.2 a	544±43 a	4.2±0.3 a	74±3 b	211±10 a	309±10 ab
		PCK	-13.6±0.5 b	5.4±0.2 b	14.9±0.4 b	25.5±1.2 b	1.7±0.3 a	370±49 a	4.5±0.2 a	81±1 a	214±17 a	363±15 b
	Type (p)		***	***	***	**	ns(0.08)	ns(0.072)	*	**	ns	*

For each species data are the mean±SE of at least N=3 biological samples assayed in duplicate. One-way ANOVA was undertaken using the photosynthetic type/subtype as the main factor. Symbols show the statistical significance levels (ns = $p > 0.05$; * = $p < 0.05$; ** = $p < 0.01$; ***: $p < 0.001$), while letters show the ranking of the means using a post hoc Tukey test (different letters indicate statistical differences at the 5% level, $p < 0.05$). k_{cat}^{o}, maximal oxygenation rate calculated from $S_{C/O} = (k_{cat}^{c} /K_C)/(k_{cat}^{o} /K_O)$. $K_C^{21\%O2}$, K_C under ambient atmospheric O_2 levels (O = 252 µM O_2 in air saturated H_2O) calculated as $K_C(1+O/K_O)$. n.m, not measured.

Table S2: The catalytic parameters of Paniceae and tobacco Rubisco between 10°C and 37°C.

Temp (°C)	**tobacco** *N* = 4 *(x2)*	*P. bis.* *N* = 3 *(x2)*	*P. milioi.* *N* = 3 *(x2)*	**C2/C3**	*P. miliac* *N* = 4 *(x2)*	*P. color* *N* = 3 *(x2)*	*P. virg* *N* = 3 *(x2)*	**NAD ME**	*P. mont.* *N* = 4 *(x2)*	*S. virid* *N* = 3 *(x2)*	*Boyd et. al 2015	*C. cilaris* *N* = 3 *(x2)*	**NADP ME**	*P. deust* *N* = 4 *(x2)*	*M. max* *N* = 3 *(x2)*	*U. panic* *N* = 3 *(x2)*	**PCK**
	k_{cat}^C (s^{-1})																
10	**0.88±0.19**	0.53±0.04	0.49±0.04	**0.51±0.02**	0.44±0.01	0.97±0.06	0.96±0.08	**0.79±0.17**	1.52±0.06	1.70±0.03	*0.88±0.08*	1.81±0.14	**1.68±0.08**	1.40±0.02	1.75±0.04	1.58±0.11	**1.58±0.10**
15	**1.37±0.22**	1.09 ±0.07	0.92±0.15	**1.00 ±0.08**	0.79±0.06	1.70±0.09	1.48±0.24	**1.32±0.27**	2.64±0.27	2.80±0.15	*1.55±0.23*	2.99±0.17	**2.81±0.10**	2.21±0.05	2.80±0.10	2.75±0.14	**2.59±0.19**
20	**1.98±0.13**	1.47±0.02	1.34±0.07	**1.40±0.07**	1.26 ±0.01	2.43±0.24	2.27±0.29	**1.99±0.37**	3.54±0.37	3.88±0.24	*3.47±0.17*	4.15±0.31	**3.86±0.18**	3.42±0.31	3.65±0.02	3.64±0.50	**3.57±0.08**
25	**3.10±0.08**	2.60±0.19	2.21±0.09	**2.41±0.20**	2.08±0.05	3.41±0.09	3.30±0.06	**2.93±0.43**	5.28±0.16	5.85±0.33	*5.21±0.22*	5.98±0.09	**5.70±0.21**	4.96±0.32	5.38±0.12	5.60±0.26	**5.28±0.18**
30	**3.78±0.37**	2.83±0.07	2.87±0.41	**2.85±0.02**	2.37±0.12	3.70±0.11	3.87±0.26	**3.31±0.48**	6.29±0.51	6.65±0.29	*8.33±2.82*	7.04±0.87	**6.66±0.22**	5.80±0.28	6.34±0.13	6.59±0.51	**6.25±0.23**
37	**5.45±0.67**	4.26±0.30	4.15±0.47	**4.20±0.06**	3.24±0.24	4.86±0.77	5.34±0.90	**4.48±0.64**	8.49±1.03	8.78±0.28	*13.88±1.35* *(35°C)*	9.01±1.21	**8.76±0.15**	7.64±0.43	7.76±0.16	8.51±0.71	**7.97±0.27**
	$K_C^{21\%O2}$ (µM)																
10	**7.6±1.9**	5.9±0.1	7.7±2.2	**6.8±0.9**	4.9±1.0	10.4±1.5	11.8±3.9	**9.0±2.1**	11.0±2.1	19.8±2.3	*35.4±5.5*	18.6±0.4	**16.5±2.8**	14.1±2.8	17.8±0.5	11.7±1.1	**14.6±1.8**
15	**11.0±1.4**	9.3±2.6	8.4±0.4	**8.8±0.5**	9.8±0.6	15.2±1.3	19.7±1.4	**14.9±2.8**	15.8±4.5	24.6±3.2	*37.9±6.7*	26.1±0.8	**22.2±3.2**	19.5±2.1	21.6±0.3	18.2±0.4	**19.8±1.0**
20	**12.9±2.0**	8.3±0.6	9.2±1.2	**8.8±0.5**	7.5±0.2	13.2±1.6	15.9±1.0	**12.2±2.5**	18.4±4.3	20.0±2.4	*50.6±7.0*	23.6±1.5	**20.7±1.5**	20.1±2.8	18.8±0.3	16.6±0.1	**18.5±1.0**
25	**18.3±0.9**	12.6±1.0	12.1±0.8	**12.4±0.3**	13.1±1.1	17.3±1.7	24.5±2.1	**18.3±3.3**	26.6±4.0	25.5±2.0	*57.5±6.3*	29.2±2.3	**27.1±1.1**	28.1±2.0	27.1±1.1	24.1±1.0	**26.4±1.2**
30	**22.0±3.4**	13.6±1.2	14.4±1.4	**14.0±0.4**	15.7±2.5	19.1±2.3	30.1±3.7	**21.9±4.6**	31.7±4.8	30.6±2.0	*103.8±9.4*	35.4±5.4	**32.6±1.5**	32.5±2.3	33.9±2.3	28.2±2.2	**31.5±1.7**
37	**30.8±3.8**	20.6±5.3	19.2±01.5	**19.9±0.8**	19.6±5.3	25.1±6.0	45.9±3.3	**30.2±8.0**	45.8±5.4	39.3±3.6	*138.1±15.3* *(35°C)*	45.6±7.2	**43.5±2.1**	42.0±3.0	39.2±2.0	38.0±6.6	**39.7±1.2**
	k_{cat}^C / $K_C^{21\%O2}$ (mM^{-1}.s^{-1})																
10	**111**	90	64	**77±13**	90	93	81	**88±4**	138	86	*26*	97	**107±16**	99	98	135	**111±12**
15	**125**	117	110	**114±3**	81	111	75	**89±11**	167	114	*42*	115	**132±17**	113	129	152	**131±11**
20	**154**	178	144	**161±17**	167	185	142	**165±12**	192	194	*73*	176	**189±6**	170	194	219	**194±14**
25	**169**	206	183	**194±12**	159	197	135	**164±18**	198	229	*93*	205	**211±9**	177	195	232	**201±16**
30	**172**	208	200	**203±4**	151	194	125	**156±20**	198	217	*81*	199	**205±6**	179	187	234	**200±17**
37	**177**	206	217	**211±5**	165	194	116	**158±23**	186	223	*104* *(35°C)*	198	**202±11**	182	198	224	**201±12**
	$S_{C/O}$ (mol.mol^{-1})																
	N = 4 *(x3)*	*N* = 2 *(x3)*	*N* = 2 *(x3)*		*N* = 2 *(x3)*	*N* = 3 *(x3)*	*N* = 2 *(x3)*			*N* = 2 *(x3)*		*N* = 2 *(x3)*		*N* = 3 *(x3)*	*N* = 2 *(x3)*	*N* = 2 *(x3)*	
10	**130.0±1.0**	152.7±2.0	152.4±4.9	**152.5±0.1**	127.1±2.6	138.2±5.1	142.7±2.6	**136.0±4.7**	n.m.	115.9±3.3	*74.9±3.6*	106.4±0.8	**111.2±3.9**	128.0±6.4	119.0±2.9	128.6±2.0	**125.2±3.1**
15	**114.7±2.1**	126.1±2.4	120.8±0.8	**123.4±2.7**	114.7±2.6	109.3±0.8	117.5±1.4	**113.8±2.4**		108.0±2.2	*74.5±9.1*	93.2±0.8	**100.6±6.0**	117.7±2.0	103.4±3.3	106.5±1.6	**109.2±4.3**
20	**94.9±0.4**	102.0±0.6	105.1±1.2	**103.5±1.6**	105.7±8.4	90.1±1.9	95.4±0.5	**97.0±4.6**		79.1±0.5	*64.1±7.9*	79.9±0.1	**79.5±0.3**	100.3±1.3	90.7±0.5	86.7±2.4	**92.6±4.0**
25	**82.0±0.6**	87.7±1.5	92.3±1.0	**90.0±2.3**	80.0±4.3	78.8±0.8	82.6±3.3	**80.4±1.1**		72.7±0.2	*61.5±2.5*	69.9±2.0	**71.3±1.2**	84.8±0.2	80.3±2.8	78.2±0.3	**81.1±1.9**
30	**69.0±2.1**	68.6±1.4	67.7±1.4	**68.2±0.4**	67.0±0.6	70.2±0.9	74.3±0.2	**70.5±2.1**		64.2±1.1	*35.6±2.0*	60.6±0.1	**62.4±1.3**	75.7±0.3	60.9±2.4	69.0±0.6	**68.5±4.3**
35	**61.1±0.7**	53.7±3.2	58.1±1.7	**55.9±2.2**	46.1±3.4	59.4±0.3	61.2±1.1	**55.6±4.8**		47.1±2.2	*27.8±3.4*	52.8±0.5	**49.9±2.3**	62.9±0.7	56.9±0.8	58.0±1.4	**59.3±1.8**

Rubisco catalysis parameters (average ± S.E.) measured in duplicate *(x2)* or triplicate *(x3)* for each biological sample (*N*). *Data for *S. viridis* Rubisco shown in blue italic (N=4 ± S.E.) measured by MIMS [15]. The data for each species are plotted in Figures S1 to S4 with the parameter averages (± SE) for tobacco Rubisco and for each Paniceae photosynthetic type/subtype shown in bold and shaded grey are plotted in Figures 3. n.m, not measured. The data from this study are statistically analyzed following derivation of the heat of activation (ΔH_a) and scaling constant (c) values for each parameter (see Table S3).

Table S3. Heat of activation (ΔH_a) and scaling constant (c) values among Paniceae and tobacco Rubisco kinetic parameters.

Species	Physiology	k_{cat}^{c} (>25°C)		k_{cat}^{c} (<25°C)		$K_C^{21\% O2}$		$S_{C/O}$	
		ΔH_a (± S.D)	c (± S.D)	ΔH_a (± S.D)	c (± S.D)	ΔH_a (± S.D)	c (± S.D)	ΔH_a (± S.D)	c (± S.D)
		$kJ.mol^{-1}$		$kJ.mol^{-1}$		$kJ.mol^{-1}$		$kJ.mol^{-1}$	
Nicotiana tabacum	C_3	36.4±2.9	15.8±1.2	60.3±1.9	25.5±0.8	37.3±1.4	17.9±0.7	22.5±1.2	-4.7±0.3
Panicum bisulcatum		32.4±8.5	13.9±3.7	71.2±7.2	29.7±3.0	31.0±3.7	15.0±1.8	29.7±2.0	-7.6±0.5
Panicum milioides	C_2	40.3±0.5	17.0±0.2	68.4±4.2	28.4±1.8	25.4±1.9	12.7±1.0	27.6±3.0	-6.7±0.7
Panicum monticola	C_4 (NADP-ME	30.6±1.8	14.0±0.8	56.5±4.2	24.5±1.8	33.8±1.9	16.9±0.9	n.m	
Cenchrus ciliaris		26.3±0.7	12.4±0.3	54.9±3.1	23.9±1.3	22.1±2.4	12.4±1.3	20.3±0.5	-4.0±0.1
Setaria viridis		26.3±2.8	12.4±1.3	56.6±2.8	24.6±1.2	21.4±0.1	11.9±0.1	25.3±4.4	-6.0±1.0
	#Boyd et al 2015	*75.0±1.1*	*31.9±0.5*	*94.2±10.4*	*39.3±9.4*	*44.7±3.8*	*22.3±1.9*	*25.2±5.7*	*-6.2±1.4*
Panicum virgatum	C_4 (NAD-ME)	31.1±2.9	13.7±1.3	58.1±0.8	24.7±0.3	34.0±4.5	16.9±2.2	23.8±1.9	-5.2±0.4
Panicum milliaceum		28.6±4.0	12.3±1.7	71.6±1.8	29.6±0.7	34.9±5.8	16.6±2.7	28.6±6.1	-7.2±1.5
Panicum coloratum		23.2±4.5	10.6±2.1	58.3±4.6	24.8±1.9	21.3±2.8	11.4±1.5	23.5±2.3	-5.1±0.5
Megathyrsus maximus	C_4 (PCK)	24.5±1.2	11.6±0.5	50.2±3.3	21.9±1.4	22.2±3.0	12.3±1.7	22.2±3.3	-4.6±0.7
Urochloa panicoides		26.9±0.9	12.6±0.4	57.3±4.5	24.8±1.9	29.9±3.0	15.2±1.5	22.3±2.0	-4.6±0.4
Panicum deustum		27.8±1.7	12.8±0.8	59.5±1.3	25.6±0.5	28.7±1.7	14.9±0.9	20.8±2.3	-3.9±0.4
Averages	C_3/C_2	36.3 b	15.5 b	69.8 b	29.0 b	28.2 a	13.9 a	28.6 b	-7.1 a
	NAD-ME	27.6 ab	12.2 a	62.7 ab	26.6 ab	30.0 a	15.0 a	25.3 ab	-5.8 ab
	NADP-ME	27.7 a	12.9 a	56.0 a	24.4 a	25.8 a	13.7 a	22.8 a	-5.0 b
	PCK	26.4 a	12.3 a	55.6 a	24.1 a	26.9 a	14.1 a	21.7 a	-4.4 b
Type (p)		ns(0.081)	ns(0.10)	*	ns(0.062)	ns	ns	ns(0.072)	ns(0.089)

Values of ΔH_a and c were determined from measures of k_{cat}^{c} (Fig S1), $K_C^{21\%O2}$ (Fig S2) and $S_{C/O}$ (Fig S4) made at 10, 15, 20, 25, 30 and 35 (or 37)°C (see Table S2 for data) and fitted to the Arrhenius-type equation

$$Parameter = exp\left[c - \frac{\Delta H_a}{RT}\right]$$

where R the molar gas constant (8.314 J K^{-1} mol^{-1}) and T the assay temperature (K). n.m, not measured. For each species data are the mean ± SE of at least N=3 biological samples assayed in duplicate. One-way ANOVA was undertaken using the photosynthetic type/subtype as the main factor. Symbols show the statistical significance levels (ns = $p > 0.05$; * = $p < 0.05$), while letters show the ranking of the means using a post hoc

Tukey test (different letters indicate statistical differences at the 5% level, $p < 0.05$). # Comparative data for *S. viridis* Rubisco from Boyd et al., (2015) [15] measured by MIMS.

Table S4. Summary of parameters used in the modelling plots shown in Figure 4 and Figure S5.

		Temperature (ºC)						
Species	**Parameters**	**10**	**15**	**20**	**25**	**30**	**37**	**Reference**
Nicotiana tabacum	$k_{cat}{}^{c}$,(s^{-1})	1.4	1.8	2.4	3.1	4.7	8.0	Tables S1-2
	$K_C{}^{air}$ (μM)	7.9	10.4	13.6	17.6	22.5	31.4	Tables S1-2
	$S_{C/O}$ (M M^{-1})	131	111	95	81	70	57	Tables S1-2
	J_{max}/V_{cmax}	2.6	2.1	1.8	1.6	1.4	1.2	Sharkey *et al.* (2007) [27]
Panicum bisulcatum	$k_{cat}{}^{c}$,(s^{-1})	1.2	1.6	2.0	2.6	4.2	8.0	Tables S1-2
	$K_C{}^{air}$ (μM)	6.2	7.8	9.7	12.1	14.8	19.6	Tables S1-2
	$S_{C/O}$ (M M^{-1})	156	125	101	83	68	52	Tables S1-2
Panicum deustum	$k_{cat}{}^{c}$,(s^{-1})	2.7	3.3	4.1	5.1	7.6	12.9	Tables S1-2
	$K_C{}^{air}$ (μM)	14.6	18.1	22.2	27.1	32.8	42.4	Tables S1-2
	$S_{C/O}$ (M M^{-1})	132	114	98	85	74	61	Tables S1-2
Urochloa panicoides	$k_{cat}{}^{c}$,(s^{-1})	3.2	3.8	4.7	5.6	8.3	13.9	Tables S1-2
	$K_C{}^{air}$ (μM)	12.5	15.5	19.2	23.6	28.8	37.6	Tables S1-2
	$S_{C/O}$ (M M^{-1})	125	106	91	78	67	55	Tables S1-2
Common parameters	g_m (mol m^{-2} s^{-1} bar^{-1})	0.24	0.33	0.44	0.57	0.72	0.97	von Caemmerer and Evans (2015) [49]
	TPU (μmol m^{-2} s^{-1})	3.81	5.62	8.14	11.40	14.65	14.10	Sharkey *et al.* (2007) [27]
	R_d (μmol m^{-2} s^{-1})	0.37	0.52	0.73	1.04	1.36	2.06	Sharkey *et al.* (2007) [27]
	s_c (M bar^{-1})	0.0512	0.0442	0.0383	0.0334	0.0292	0.0245	https://en.wikipedia.org/wiki/Henry's_law
	s_o (M bar^{-1})	0.00170	0.00154	0.00139	0.00126	0.00115	0.00101	https://en.wikipedia.org/wiki/Henry's_law
	J_{max} (μmol m^{-2} s^{-1})	63	87	118	160	214	317	Sharkey *et al.* (2007) [27]
	Rubisco sites (μmol s^{-1})	30	30	30	30	30	30	

Photosynthesis rate, A was calculated as $A = \min(A_c, A_j, A_t)$, where A_c, A_j and A_t are the CO_2-limited (A_c), light-limited (A_j) and the triose phosphate utilisation (TPU)-limited (A_t) assimilation rates, respectively. Their expressions are defined as:

$$A_c = \frac{m.k_{\text{cat}}{}^{c}\left(C_c.s_c - 0.5O_c/S_{c/o}\right)}{\left(C_c.s_c + K_{c\text{air}}\right)} - R_d\ ;$$

$A_j = \frac{(C_c.s_c - 0.5O_c/S_{c/o})J_{\max}}{4(C_c.s_c + O_c/S_{c/o})} - R_d$; and

$A_t = 3\mathrm{TPU} - R_d$.

The model parameters used are: m = amount of leaf Rubisco set at 30 µmol active sites m^{-2}; $k_{\mathrm{cat}}{}^{c}$ (s^{-1}) = Rubisco carboxylation rate; $K_{\mathrm{C}}{}^{\mathrm{air}}$ (µM) = Michaelis-Menten constant of Rubisco for CO_2 and $S_{C/O}$ = CO_2/O_2 specificity of Rubisco. The maximal RuBP carboxylation-limited assimilation rate, V_{cmax} = m.$k_{\mathrm{cat}}{}^{c}$. The maximal RuBP regeneration-limited assimilation rate, $J_{\max}$ (µmol m^{-2} s^{-1}) is set to equal 1.7V_{cmax} for tobacco at 25°C; its values at other temperatures were calculated using the thermal dependence from Bernacchi et al (2003) [50]:

$J_{max}(T) = J_{max_{25}} \cdot e^{\left(c - \frac{Ha}{R.(273+T)}\right)}$, where c = 17.7 and ΔH_a = 43.9 (in kJ mol^{-1}).

The values at 25°C for TPU (11.4 µmol m^{-2} s^{-1}) and mitochondrial respiration, R_d (1 µmol m^{-2} s^{-1}) and their thermal dependence were adapted from Sharkey et al (2007) [27]:

$R_d(T) = R_{d_{25}} \cdot e^{\left(c - \frac{Ha}{R.(273+T)}\right)}$, where c = 18.72 and ΔH_a = 46.4 (in kJ mol^{-1})

$TPU(T) = TPU_{25}\left[\frac{e^{\left(c - \frac{Ha}{R.(273+T)}\right)}}{1+e^{\left(\frac{S.(273+T).Hd}{R.(273+T)}\right)}}\right]$, where c =21.46 and ΔH_a = 53.1, ΔH_d = 201.8 and 0.65 (in kJ mol^{-1}).

C_c and O_c are the CO_2 and O_2 concentrations in the chloroplast, respectively. Gas concentrations in the liquid phase were calculated using the solubility constants for CO_2 (s_c = 0.0334 M bar^{-1}) and O_2 (s_o = 0.00126 M bar^{-1}) at 25^{o}C. Their thermal dependence was determined according to Henry's law using the following expressions (https://en.wikipedia.org/wiki/Henrys_law):

$$s_c(T) = s_{c_{25}} \cdot 2400.e^{\left(\frac{1}{273+T} - \frac{1}{298}\right)}$$ and

$$s_o(T) = s_{o_{25}} \cdot 1700.e^{\left(\frac{1}{273+T} - \frac{1}{298}\right)}$$

Intercellular CO_2 concentration, C_i was calculated using a constant C_i/C_a ratio of 0.70[49]. C_c was calculated as $C_c = C_i - A/g_m$, where g_m is the mesophyll conductance to CO_2 transfer. Tobacco g_m at 25^{o}C (0.57 mol m^{-2} s^{-1} bar^{-1}) and its thermal dependence were taken from von Caemmerer and Evans (2015) [49].

Table S5. Parameters used to calculate CO_2 concentrations in $^{14}CO_2$-fixation assays at the varying temperatures.

Parameter (*units*)	Value					
T; assay temperature	(10°C) 283K	(15°C) 288K	(20°C) 293K	(25°C) 298K	(30°C) 303K	(37°C) 310K
q; CO_2 solubility at 1 atm ($Mol.L^{-1}.atm^{-1}$)	0.0524	0.0455	0.0382	0.0329	0.0289	0.0240
R: universal gas constant ($L.atm.K^{-1}.mol^{-1}$)	0.082057					
pK_1	6.362	6.327	6.280	6.251	6.226	6.202
pK_2	10.499	10.431	10.377	10.329	10.290	10.238
*pH	8.27	8.24	8.21	8.16	8.11	8.03

The values were fitted to the Henderson-Hasselbalch derived equation

$$[CO_2] = \frac{(C_t)}{1 + \frac{V}{vqRT} + 10^{(pH-pK1)} + 10^{(2pH-pK1-pK2)}}$$

V/v: ratio of reaction vial headspace (*V*) to assay volume (*v*).

*example pH variation for 50 mM EPPES-NaOH buffer adjusted to pH 8.16 at 25°C; the 0.26 pH variation has <1% effect on tobacco Rubisco carboxylase activity.

References

1 Andrews, T. J. & Whitney, S. M. Manipulating ribulose bisphosphate carboxylase/oxygenase in the chloroplasts of higher plants. *Arch.Biochem.Biophys.* **414**, 159-169 (2003).

2 Carmo-Silva, E., Scales, J. C., Madgwick, P. J. & Parry, M. A. J. Optimizing Rubisco and its regulation for greater resource use efficiency. *Plant Cell Env* **38**, 1817-1832 (2015).

3 Raven, J. A. Rubisco: still the most abundant protein of Earth? *New Phytol* **198**, 1-3 (2013).

4 Sage, R. F. The evolution of C_4 photosynthesis *New Phytol* **161**, 341-370 (2004).

5 Sage, R. F., Christin, P.-A. & Edwards, E. J. The C_4 plant lineages of planet Earth. *J Exp Bot* **62**, 3155-3169 (2011).

6 Furbank, R. T. Evolution of the C_4 photosynthetic mechanism: are there really three C_4 acid decarboxylation types? *J Exp Bot* **62**, 3103-3108 (2011).

7 Sage, R. F., Sage, T. L. & Kocacinar, F. Photorespiration and the evolution of C_4 photosynthesis. *Ann Rev Plant Biol* **63**, 19-47 (2012).

8 Sharwood, R. E., Ghannoum, O. & Whitney, S. M. Prospects for improving CO_2 fixation in C_3-crops through understanding C_4-Rubisco biogenesis and catalytic diversity. *Currt Opin Plant Biol* **31**, 135-142 (2016).

9 Ghannoum, O. *et al.* Faster rubisco is the key to superior nitrogen-use efficiency in NADP-malic enzyme relative to NAD-malic enzyme C_4 grasses. *Plant Physiol* **137**, 638-650 (2005).

10 von Caemmerer, S., Quick, W. P. & Furbank, R. T. The development of C_4 rice: current progress and future challenges. *Science* **336**, 1671-1672 (2012).

11 Sharwood, R., von Caemmerer, S., Maliga, P. & Whitney, S. The catalytic properties of hybrid Rubisco comprising tobacco small and sunflower large subunits mirror the kinetically equivalent source Rubiscos and can support tobacco growth. *Plant Physiol* **146**, 83-96 (2008).

12 Sharwood, R. E., Sonawane, B. V., Ghannoum, O. & Whitney, S. M. Improved analysis of C_4 and C_3 photosynthesis via refined in vitro assays of their carbon fixation biochemistry. *J Exp Bot* **67**, 3137-3148 (2016).

13 Whitney, S. M. & Sharwood, R. E. Construction of a tobacco master line to improve Rubisco engineering in chloroplasts. *J Exp Bot* **59**, 1909-1921 (2008).

14 Tcherkez, G. G. B., Farquhar, G. D. & Andrews, T. J. Despite slow catalysis and confused substrate specificity, all ribulose bisphosphate carboxylases may be nearly perfectly optimized. *Proc Nat Acad Sci* **103**, 7246-7251 (2006).

15 Boyd, R. A., Gandin, A. & Cousins, A. B. Temperature response of C_4 photosynthesis: biochemical analysis of Rubisco, phosphoenolpyruvate carboxylase and carbonic anhydrase in *Setaria viridis*. *Plant Physiol* **169**, 1850-1861 (2015).

16 Carmo-Silva, A. E. *et al.* Rubisco activities, properties, and regulation in three different C_4 grasses under drought. *J Exp Bot* **61**, 2355-2366 (2010).

17 Galmes, J. *et al.* Expanding knowledge of the Rubisco kinetics variability in plant species: environmental and evolutionary trends. *Plant Cell Environ* **37**, 1989-2001 (2014).

18 Galmés, J., Kapralov, M. V., Copolovici, L. O., Hermida-Carrera, C. & Niinemets, Ü. Temperature responses of the Rubisco maximum carboxylase activity across domains of life: phylogenetic signals, trade-offs, and importance for carbon gain. *Photosynth Res* **123**, 183-201 (2015).

19 Perdomo, J. A., Cavanagh, A. P., Kubien, D. S. & Galmés, J. Temperature dependence of in vitro Rubisco kinetics in species of *Flaveria* with different photosynthetic mechanisms. *Photosynth Res* **124**, 67-75 (2015).

20 Sage, R. F. Variation in the k_{cat} of Rubisco in C_3 and C_4 plants and some implications for photosynthetic performance at high and low temperature. *J Exp Bot* **53**, 609-620 (2002).

21 Savir, Y., Noor, E., Milo, R. & Tlusty, T. Cross-species analysis traces adaptation of Rubisco toward optimality in a low-dimensional landscape. *Proc Nat Acad Sci* **107**, 3475-3480 (2010).

22 Pearcy, R. W. & Ehleringer, J. Comparative ecophysiology of C_3 and C_4 plants. *Plant Cell Env* **7**, 1-13 (1984).

23 Tcherkez, G. The mechanism of Rubisco-catalyzed oxygenation. *Plant Cell Env* **39**, 983-997 (2016).

24 Farquhar, G. D., von Caemmerer, S. & Berry, J. A. A biochemical model of photosynthetic CO_2 assimilation in leaves of C_3 species. *Planta* **149**, 78-90 (1980).

25 Sharwood, R. E. & Whitney, S. M. Correlating Rubisco catalytic and sequence diversity within C_3 plants with changes in atmospheric CO_2 concentrations. *Plant Cell Env* **37**, 1981-1984 (2014).

26 Young, J. N. *et al.* Large variation in the Rubisco kinetics of diatoms reveals diversity among their carbon-concentrating mechanisms. *J Exp Bot* **67**, 3445-3456 (2016).

27 Sharkey, T. D., Bernacchi, C. J., Farquhar, G. D. & Singsaas, E. L. Fitting photosynthetic carbon dioxide response curves for C_3 leaves. *Plant Cell Env* **30**, 1035-1040 (2007).

28 Walker, B., Ariza, L. S., Kaines, S., Badger, M. R. & Cousins, A. B. Temperature response of *in vivo* Rubisco kinetics and mesophyll conductance in *Arabidopsis thaliana*: comparisons to *Nicotiana tabacum*. *Plant Cell Env* **36**, 2108-2119 (2013).

29 Whitney, S. M., Houtz, R. L. & Alonso, H. Advancing our understanding and capacity to engineer nature's CO_2-sequestering enzyme, Rubisco. *Plant Physiol* **155**, 27-35 (2011).

30 Hermida-Carrera, C., Kapralov, M. V. & Galmés, J. Rubisco catalytic properties and temperature response in crops. *Plant Physiol.*, doi:10.1104/pp.16.01846 (2016).

31 Orr, D. *et al.* Surveying Rubisco diversity and temperature response to improve crop photosynthetic efficiency. *Plant Physiol.*, doi:10.1104/pp.16.00750 (2016).

32 Badger, M. R. & Collatz, G. J. Studies on the kinetic mechanism of RuBP carboxylase and oxygenase reactions, with particular reference to the effect of temperature on kinetic papameters. *Carnegie YB* **76**, 355-361 (1977).

33 Jordan, D. B. & Ogren, W. L. The CO_2/O_2 specificity of ribulose 1,5-bisphosphate carboxylase oxygenase - dependence on ribulosebisphosphate concentration, pH and temperature. **161**, 308-313 (1984).

34 Ishikawa, C., Hatanaka, T., Misoo, S., Miyake, C. & Fukayama, H. Functional incorporation of sorghum small subunit increases the catalytic turnover rate of Rubisco in transgenic rice *Plant Physiol* **156**, 1603-1611 (2011).

35 Prins, A. *et al.* Rubisco catalytic properties of wild and domesticated relatives provide scope for improving wheat photosynthesis. *J Exp Bot* **67**, 1827-1838 (2016).

36 Hauser, T., Popilka, L., Hartl, F. U. & Hayer-Hartl, M. Role of auxiliary proteins in Rubisco biogenesis and function. *Nat Plants* **1** (2015).

37 Wachter, R. M. *et al.* Activation of interspecies-hybrid Rubisco enzymes to assess different models for the Rubisco-Rubisco activase interaction. *Photosynth Res* **117**, 557-566 (2013).

38 Andersson, I. & Backlund, A. Structure and function of Rubisco. *Plant Physiol Biochem* **46**, 275-291 (2008).

39 Spreitzer, R. J., Peddi, S. R. & Satagopan, S. Phylogenetic engineering at an interface between large and small subunits imparts land-plant kinetic properties to algal Rubisco. *Proc Natl Acad Sci* **102**, 17225-17230 (2005).

40 Andersson, I. Catalysis and regulation in Rubisco. *J Exp Bot* **59**, 1555-1568 (2008).

41 von Caemmerer, S. & Furbank, R. T. The C_4 pathway: an efficient CO_2 pump. *Photosynth Res* **77**, 191-207, doi:10.1023/a:1025830019591 (2003).

42 Still, C. J., Pau, S. & Edwards, E. J. Land surface skin temperature captures thermal environments of C_3 and C_4 grasses. *Glob Ecol Biogeo* **23**, 286-296 (2014).

43 Galmés, J. *et al.* Environmentally driven evolution of Rubisco and improved photosynthesis and growth within the C_3 genus *Limonium* (Plumbaginaceae). *New Phytol* **203**, 989-999 (2014).

44 Whitney, S. M. & Andrews, T. J. Plastome-encoded bacterial ribulose-1, 5-bisphosphate carboxylase/oxygenase (RubisCO) supports photosynthesis and growth in tobacco. *Proc Nat Acad Sci* **98**, 14738-14743 (2001).

45 Parry, M. A. J. *et al.* Rubisco activity and regulation as targets for crop improvement. *J Exp Bot* **64**, 717-730 (2013).

46 Bortesi, L. & Fischer, R. The CRISPR/Cas9 system for plant genome editing and beyond. *Biotech Adv* **33**, 41-52 (2015).

47 Stamatakis, A. RAxML version 8: a tool for phylogenetic analysis and post-analysis of large phylogenies. *Bioinform* **30**, 1312-1313 (2014).

48 Whitney, S. M., Birch, R., Kelso, C., Beck, J. L. & Kapralov, M. V. Improving recombinant Rubisco biogenesis, plant photosynthesis and growth by coexpressing its ancillary RAF1 chaperone. *Proc Natl Acad Sci* **112**, 3564-3569 (2015).

49 von Caemmerer, S. & Evans, J. R. Temperature responses of mesophyll conductance differ greatly between species. *Plant Cell Env* **38**, 629-637 (2015).

50 Bernacchi, C. J., Pimentel, C. & Long, S. P. In vivo temperature response functions of parameters required to model RuBP-limited photosynthesis. *Plant Cell Env* **26**, 1419-1430 (2003).